

Simulation of Stochastic Volatility using Path Integration: Smiles and Frowns

Belal E. Baaquie ¹, L.C. Kwek and M. Srikant
*Department Of Physics, National University of Singapore,
Kent Ridge, Singapore 119260*

Abstract

We apply path integration techniques to obtain option pricing with stochastic volatility using a generalized Black-Scholes equation known as the Merton and Garman equation. We numerically simulate the option prices using the technique of path integration. Using market data, we determine the parameters of the model. It is found that the market chooses a special class of models for which a more efficient algorithm, called the bisection method, is applicable. Using our simulated data, we generate some implied volatility curves. We also analyze and study in detail some of the characteristics of the volatility curves within the model.

¹Email:phybeb@nus.edu.sg

1 Introduction

Two popular instruments for option valuation in the market are the binomial option pricing and the Black-Scholes model [4]. The underlying stochastic nature of these models resembles quantum mechanical theories. In quantum mechanics, tools have been invented to solve and compute such stochastic quantities; one widely used instrument in this field is an intriguing integral called the path integration. The application of this method to option pricing has been mooted and elucidated in great detail in elsewhere [1]. The underlying principle behind the method is essentially based on a generalized Black-Scholes model but unlike the Black-Scholes model, the new formalism can easily accommodate stochastic volatility and provide wider scope and greater flexibility for the investigation of market behavior.

The most direct advantage of recasting the option pricing problem in terms of this Feynman path integral is that this formalism allows a new perspective for the trader and market analysts, and can lead to several new ways of computing exact, approximate and numerical solutions for the pricing of option. Stochastic volatility is naturally incorporated within the model. Stochastic volatility can introduce a high degree of nonlinearity within the option pricing problem. The path integral formalism can in principle handle such nonlinearity in an elegant manner. Moreover, there is a possibility that traders who are learnt this new tool can formulate new exotic options.

There are many inherent similarities between the problem of pricing options in finance and solution of models in the physical sciences using stochastic approach. Indeed, this striking similarity have prompted Bouchaud and others [6, 8, 26] to apply successfully many mathematical tools previously used by physicists, like functional integration and scale invariance, to analyze problems in the financial markets.

The celebrated Black-Scholes equation provides a simple and analytical formula for traders interested in plain vanilla European option. Equipped with the formula, analysis of the simplest option simply involves taking parameters estimated from historical data and working out the price of the option. Nowadays, even in the simplest scenario, market analysts utilize option pricing using Black-Scholes formula with a twist. Instead of estimating the constant volatility required in Black-Scholes equation, which is often difficult and inaccurate, they usually compute the implied volatility which is necessary for the traded option price for a specific strike price to be consistent with the Black-Scholes formula. Such an analysis gives rise to a graph of implied volatility against strike price which normally ap-

pears as a smile or a frown. The decision regarding various investment portfolios depends largely on the difference between this implied volatility and the historical volatility. Large implied volatility is taken by traders to mean that the option is overpriced.

Numerous extensions on the Black-Scholes model have been proposed, see for instance Wilmott's book on financial derivatives [?] and references therein. Moreover, to explain the deviation of the call option from the Black-Scholes model, many refinements to the original model have been studied. For instance, one possible refinement is to relax the fixed volatility rate and replace it with stochastic volatility. Another refinement is to consider the stochastic model for the pricing of the security as a jump-diffusion process [10, 17]. Recently, it has been shown by Das and Sundaram [11] that certain securities which follow a jump-diffusion process can exhibit stochastic volatility. There are essential differences between the last two examples of possible refinements. For the jump-diffusion case, the effect is enhanced within short terms whereas for stochastic volatility, the effect is more pronounced over a longer maturity time. Finally, one can also combine the two effects and consider stochastic interest rates.

Constructing models for option pricing with stochastic volatility is an important issue since there are strong indications of stochastic variations in the underlying asset pricing and their derivatives from numerous empirical data. Several papers have recently attempted to study this pricing bias caused by stochastic volatility [?, 2, 11, 13, 16]. These studies have generally focused on numerical solutions of partial differential equations, Fourier inversion methods and the power series approximation techniques. The method of solving partial differential equations to study the option pricing has been considered to be the one of the general approach. However, a major distinct disadvantage of this technique is that most of the work done using this method is heavily computer intensive. The path integral formulation, on the other hand, offers an intermediate alternatives in many instances. It can include many of these techniques and offer new insights into the pricing of options. Moreover, the path integrals can yield results in a global approach involving the properties of the model at all times.

In this paper, we investigate option valuation using the path integral approach. We generate the volatility curves and study their behaviors. As the application of path integration to option pricing differs from the current theoretical method used for evaluating the option prices in the market, we shall briefly sketch the theoretical basis of our formulation in the next section. A detailed review and description of the path integral formalism in option

pricing will not be given here. A more elaborated account of the path integral formalism to option pricing can be found in the following reference [1].

In section 2, we discuss at length the theoretical framework of our model. The general algorithm using Monte Carlo techniques is given in the section 3. We perform the numerical simulations for our model in section 4 and calibrate market data to the model in the same section. We find that the market seems to choose a special set of parameters. For this set of parameters, there exist more efficient algorithm called the bisection method. In section 5, we describe this algorithms and provide the necessary pseudocodes for the bisection method. We also briefly discuss the convergence of the program.

Finally, in section 6, we briefly discuss and study some characteristics of the implied volatility curves generated. Our simulation is based on Merton and Garman equation and consequently, there are several parameters which we can vary within the model. Besides the correlation coefficient between the security prices and the volatility, our model involves two other arbitrary constants; one related to the variance and the other related to the mean of the stochastic volatility. The initial stock price and the initial volatility can also be varied and studied. Using the path integral formalism, we generate computer data on option pricing by varying the various parameters in the model. Based on the option prices, we compute the implied volatilities and analyze the graphs of implied volatility against strike price.

2 Theoretical Formulation

Black and Scholes [4] laid the foundation for a quantitative analysis of European options. Since then, several extensions have been done and some of the original assumptions have been dropped. In an important paper, Merton [23] ingeniously removed the assumption of constant interest rates and showed that an option can be priced in terms of a bond price. In the same paper, Merton also showed how the Black-Scholes formula can be extended to cover situations in which the volatility is a deterministic function of time. Indeed, based on a critical analysis of market data, Rubinstein has shown that the assumption of constant volatility is generally incorrect [29]. Research has also been done assuming different processes for the evolution of stock prices by Merton [24], Cox and Ross [9] and Jones [19]. Cox and Ross [9] and Rubinstein [28] have solved the problem for the case when the volatility is a function of the underlying security price.

Empirical evidence investigating the distribution of stock returns has shown mixed re-

sults. Kon [?] finds that the observed distributions are consistent with stochastic volatility while Scott [30] shows that the hypothesis that stock returns are distributed independently over time can be rejected. Bodurtha and Courtadon [5] and Hull and White [15] also support the hypothesis of stochastic volatility. Considering these results, it seems reasonable to model volatility as another stochastic variable.

2.1 The Stochastic Process With Volatility

Several stochastic processes for the volatility have been considered by researchers. For example, Hull and White [14], Heston [13] and others have considered the process

$$dV = (a + bV)dt + \xi V^{1/2}dz \quad (1)$$

where Q is white noise and $V = \sigma^2$. Baaquie [1], Hull and White and others have considered

$$dV = \mu V dt + \xi V dz \quad (2)$$

while Stein and Stein [?] consider

$$d\sigma = -\delta(\sigma - \theta)dt + kdz \quad (3)$$

where δ and θ are constants representing the mean reversion strength and the mean value of the volatility respectively. We see that all the processes above except for (3)² follow the general form

$$dV = (\lambda + \mu V)dt + \xi V^\alpha dz \quad (4)$$

The choice of λ and μ is restricted by the condition that $V > 0$.

2.2 The Merton-Garman Equation

The process we are considering is

$$dS = \phi S dt + \sigma S dz_1 \quad (5)$$

$$dV = (\lambda + \mu V)dt + \xi V^\alpha dz_2 \quad (6)$$

²We can include this process if we add a term of the form $\gamma V^{1/2}$ to the drift term

where ϕ , λ , μ and ξ are constants, $V = \sigma^2$ and z_1 and z_2 are Wiener processes with correlation $-1 \leq \rho \leq 1$. Using Ito's lemma, we obtain the following expression for the process followed by a derivative f_i dependent on the underlying security and the volatility of that security

$$\begin{aligned} df_i &= \left(\frac{\partial f_i}{\partial t} + \phi S \frac{\partial f_i}{\partial S} + (\lambda + \mu V) \frac{\partial f_i}{\partial V} + \frac{\sigma^2 S^2}{2} \frac{\partial^2 f_i}{\partial S^2} + \rho V^{1/2+\alpha} \xi \frac{\partial^2 f_i}{\partial S \partial V} + \frac{\xi^2 V^{2\alpha}}{2} \frac{\partial^2 f_i}{\partial V^2} \right) dt \\ &\quad + \sigma S \frac{\partial f_i}{\partial S} dz_1 + \xi V^\alpha \frac{\partial f_i}{\partial V} dz_2 \\ &= \Theta_i dt + \Xi_i dz_1 + \Psi_i dz_2 \end{aligned} \quad (7)$$

We write it in this form to separate the stochastic and non-stochastic terms.

We now consider two different options, f_1 and f_2 on the same underlying security with strike prices and maturities given by K_1 , K_2 , T_1 and T_2 respectively. We form a portfolio

$$\Pi = f_1 + \Gamma_1 f_2 + \Gamma_2 S \quad (8)$$

so that

$$d\Pi = (\Theta_1 + \Gamma_1 \Theta_2 + \Gamma_2 \phi S) dt + (\Xi_1 + \Gamma_1 \Xi_2 + \Gamma_2 \sigma S) dz_1 + (\Psi_1 + \Gamma_1 \Psi_2) dz_2 \quad (9)$$

We have to get rid of the stochastic terms to ensure perfect hedging. Hence, we set

$$\Xi_1 + \Gamma_1 \Xi_2 + \Gamma_2 \sigma S = 0 \quad (10)$$

$$\Psi_1 + \Gamma_1 \Psi_2 = 0 \quad (11)$$

to obtain

$$\Gamma_1 = -\frac{\Psi_1}{\Psi_2} = -\frac{\partial f_1 / \partial V}{\partial f_2 / \partial V} \quad (12)$$

$$\Gamma_2 = \frac{\Psi_1}{\Psi_2} \frac{\partial f_2}{\partial S} - \frac{\partial f_1}{\partial S} = \frac{\partial f_1 / \partial V}{\partial f_2 / \partial V} \frac{\partial f_2}{\partial S} - \frac{\partial f_1}{\partial S} \quad (13)$$

Since the portfolio is now risk-less, it must increase at the risk-free interest rate by the principle of no arbitrage. In other words, we must have

$$d\Pi = r\Pi dt \quad (14)$$

Expanding Π and simplifying, we obtain, after a separation of variables

$$\begin{aligned}
& \frac{1}{\partial f_1 / \partial V} \left(\frac{\partial f_1}{\partial t} + (\lambda + \mu V) \frac{\partial f_1}{\partial V} + rS \frac{\partial f_1}{\partial S} + \frac{VS^2}{2} \frac{\partial^2 f_1}{\partial S^2} \right. \\
& \quad \left. + \rho V^{1/2+\alpha} \xi \frac{\partial^2 f_1}{\partial S \partial V} + \frac{\xi^2 V^{2\alpha}}{2} \frac{\partial^2 f_1}{\partial V^2} - r f_1 \right) \\
= & \frac{1}{\partial f_2 / \partial V} \left(\frac{\partial f_2}{\partial t} + (\lambda + \mu V) \frac{\partial f_2}{\partial V} + rS \frac{\partial f_2}{\partial S} + \frac{VS^2}{2} \frac{\partial^2 f_2}{\partial S^2} \right. \\
& \quad \left. + \rho V^{1/2+\alpha} \xi \frac{\partial^2 f_2}{\partial S \partial V} + \frac{\xi^2 V^{2\alpha}}{2} \frac{\partial^2 f_2}{\partial V^2} - r f_2 \right) \equiv \beta(S, V, t, r)
\end{aligned} \tag{15}$$

It is important to note that β is not a function of K_1 , K_2 , T_1 or T_2 . This follows from the fact that the first expression is dependent only on K_1 and T_1 while the second is dependent only on K_2 and T_2 . Hence, it is independent of all four variables. The term β is referred to as the market price of volatility risk. This is because the higher the value of β , the more averse the investors are to take on the volatility risk. The reason this parameter is needed to price options with stochastic volatility and not for Black-Scholes pricing is that volatility is not traded in the market. Hence, it is not possible to perfectly hedge against the volatility even though it is possible to perfectly hedge against the underlying security price. Hence, investor risk preferences have to be considered when considering stochastic volatility or, in other words, risk-neutral valuation cannot be applied directly to volatility since volatility is not directly traded in the market.

The parameter, β , is difficult to estimate empirically and there is some evidence that it is non-zero [?]. To estimate this quantity, we consider the Cox, Ingersoll and Ross model where the consumption growth has constant correlation with the spot-asset return. This gives rise to a risk premium which is proportional to the volatility. We assume this model for simplicity as it has only the effect of redefining μ in the above equation. Henceforth, we shall assume that the market price of risk has been included in the Merton-Garman equation by redefining μ . Therefore, the Merton-Garman equation for the process we are considering is

$$\frac{\partial f}{\partial t} + rS \frac{\partial f}{\partial S} + (\lambda + \mu V) \frac{\partial f}{\partial V} + \frac{1}{2} VS^2 \frac{\partial^2 f}{\partial S^2} + \rho \xi V^{1/2+\alpha} S \frac{\partial^2 f}{\partial S \partial V} + \xi^2 V^{2\alpha} \frac{\partial^2 f}{\partial V^2} = r f \tag{16}$$

We introduce the variables $S = e^x$ and $V = e^y$ to simplify the calculations. In terms of these

variables, the Merton-Garman equation is

$$\begin{aligned} \frac{\partial f}{\partial t} + \left(r - \frac{e^y}{2}\right) \frac{\partial f}{\partial x} + \left(\lambda e^{-y} + \mu - \frac{\xi^2}{2} e^{2y(\alpha-1)}\right) \frac{\partial f}{\partial y} + \frac{e^y}{2} \frac{\partial^2 f}{\partial x^2} + \rho \xi e^{y(\alpha-1/2)} \frac{\partial^2 f}{\partial x \partial y} \\ + \xi^2 e^{2y(\alpha-1)} \frac{\partial^2 f}{\partial y^2} = r f \end{aligned} \quad (17)$$

For an option, we have $f(T) = \max(e^x - K, 0)$, T being the maturity time. Hence, this is a final value problem.

2.3 The “Straightforward” Solution when $\rho = 0$

When $\rho = 0$, the solution for any volatility process, stochastic or non-stochastic is straightforward. We make use of the theorem of Merton that the solution for a deterministic volatility process is the Black-Scholes price with the volatility variable replaced by the average volatility. We can consider the stochastic volatility case as a collection of a large number of deterministic volatility processes and the option price is then the average of the prices produced by each of the processes. In other words, if the volatility follows the generic process $V(t)$ (where V may be stochastic), the option price will be given by

$$C = \int_0^\infty [SN(d_1(V)) - Ke^{-r\tau}N(d_2(V))]V_m(V)dV \quad (18)$$

where V_m is the probability distribution function for the mean of the volatility $\frac{1}{T} \int_0^T V(t)dt$ (which is a delta function for a deterministic process) and $d_1(V)$ and $d_2(V)$ are the usual variate in Black-Scholes equation defined by $d_j = \frac{\ln(S/X) + (r + (-1)^j/2)(T - t)}{\sigma\sqrt{T - t}}$, $j = 1, 2$, K is the strike price. Here, $N(x)$ is the cumulative probability distribution function for a standardized normal variate.

This intuitive result is derived in Scott [30].

We will give two simple examples to illustrate this. First, let us consider a deterministic process. We will choose the process

$$V = V_0 e^{\mu t}, \quad 0 \leq t \leq T \quad (19)$$

In this case, the probability distribution function of the mean of the volatility is given by

$$V_m = \delta\left(V - V_0 \frac{e^{\mu T} - 1}{\mu T}\right) \quad (20)$$

giving us the Black-Scholes result with σ replaced by $\sqrt{V_0 \frac{e^{\mu T} - 1}{\mu T}}$.

For a stochastic volatility process, we choose³ $\lambda = \mu = \alpha = 0$ in eq(6) to obtain

$$dV = \xi dz, V(0) = V_0, 0 \leq t \leq T \quad (21)$$

where Q represents white noise. The distribution of the mean of V during the time interval $(0, T)$ is given by

$$V_m \sim N\left(V_0, \frac{\xi^2 T}{3}\right) \quad (22)$$

Hence, the option price is given by

$$C = \sqrt{\frac{3}{2\pi\xi^2 T}} \int_0^\infty [SN(d_1(V)) - Ke^{-r\tau} N(d_2(V))] \exp\left(-\frac{3(V - V_0)^2}{2\xi^2 T}\right) dV. \quad (23)$$

2.4 An Extension to Merton's Theorem

The case $\rho = 0$ corresponds to Merton's Theorem. We now extend Merton's theorem to the case of non-zero correlation for the stochastic process of the volatility that we are investigating. The present value of the option is given by

$$f(x, y, T) = \int_{-\infty}^\infty \langle x, y \mid e^{-\hat{H}\tau} \mid x' \rangle f(x', T) dx' \quad (24)$$

and $\langle x, y \mid e^{-\hat{H}\tau} \mid x' \rangle$ is given by equation (90) with S_0 and S_1 given by (93) and (84) respectively. Now, since $\int DY e^{S_0}$ describes the probability of a specific path for y (we show this in detail in chapter 6), we see that the propagator can now be written as in equation (89) with ω, θ, η and ζ being functionals of this path and ν being the final value of $V^{3/2-\alpha}$ for the path. Hence, if we generate paths for y according to (6), the option price is given by

$$f(x, y, t) = \left\langle \int_{\ln K}^\infty dx' \frac{e^{S_1(x, x', \omega, \theta, \eta, \zeta, \nu)}}{\sqrt{2\pi\epsilon(1-\rho^2)}} (e^{x'} - K)_+ \right\rangle \quad (25)$$

(since the payoff of the option is given by $(e^{x'} - K)_+$) with the average taken over the paths for V . Since the propagator is in the form of a Gaussian, we can perform the integration over x' to obtain

$$f(x, y, t) = \left\langle SN(s_1) \exp\left(-\frac{\rho^2}{2}\omega - \frac{\rho}{(3/2-\alpha)\xi} \left(V_i^{3/2-\alpha} - V_f^{3/2-\alpha}\right) - \frac{\rho\lambda}{\xi}\theta - \frac{\rho\mu}{\xi}\eta + \frac{\rho\xi}{2}\zeta\right) - Ke^{-r\tau} N(s_2) \right\rangle \quad (26)$$

³This is not a realistic process as $P(V < 0) > 0$ while V is obviously non-negative. However, it might be a reasonable approximation for relatively short times for which $P(V < 0)$ is negligible.

where V_i and V_f are the initial and final volatilities of the path respectively and s_1 and s_2 are given by

$$s_1 = \frac{\ln\left(\frac{S}{K}\right) + r\tau + \frac{1}{2}(1 - 2\rho^2)\omega + \frac{\rho}{(3/2-\alpha)\xi} \left(V_i^{3/2-\alpha} - V_f^{3/2-\alpha}\right) + \frac{\rho\lambda}{\xi}\theta + \frac{\rho\mu}{\xi}\eta - \frac{\rho\xi}{2}\zeta}{\sqrt{(1 - \rho^2)\omega}} \quad (27)$$

$$s_2 = s_1 - \sqrt{(1 - \rho^2)\omega} \quad (28)$$

It is easy to verify that equation (26) is the same as the Black-Scholes equation for any single volatility path when $\rho = 0$.

When $\alpha = \frac{1}{2}$, several simplifications occur. We see that $\theta = \zeta = \tau$ are known and $\eta = \omega$. In that case, (26) reduces to

$$\left\langle SN(s_1) \exp\left(-\left(\frac{\rho^2}{2} + \frac{\rho\mu}{\xi}\right)\omega - \frac{\rho}{\xi}(V_i - V_f) - \rho\left(\frac{2\lambda - \xi^2}{2\xi}\right)\tau\right) - Ke^{-r\tau}N(s_2) \right\rangle \quad (29)$$

where s_1 and s_2 now have the relatively simple forms

$$s_1 = \frac{\ln\left(\frac{S}{K}\right) + \left(r + \rho\left(\frac{2\lambda - \xi^2}{2\xi}\right)\right)\tau - \left(\rho^2 - \frac{\rho\mu}{\xi} - \frac{1}{2}\right)\omega + \frac{\rho}{\xi}(V_i - V_f)}{\sqrt{(1 - \rho^2)\omega}} \quad (30)$$

$$s_2 = s_1 - \sqrt{(1 - \rho^2)\omega} \quad (31)$$

Hence, we see that we have a straightforward solution for $\alpha = \frac{1}{2}$ even when the correlation is not zero.

When $\alpha = \frac{3}{2}$ and $\lambda = 0$, we obtain a similar simplification since $\zeta = \omega$ and $\eta = \tau$. In this case, we obtain the following expression for the option price

$$f(x, y, t) = \left\langle SN(s_1) \exp\left(-\frac{\rho}{2}\left((\rho - \xi)\omega + 2\ln\left(\frac{V_i}{V_f}\right) + 2\frac{\mu\tau}{\xi}\right)\right) - Ke^{-r\tau}N(s_2) \right\rangle \quad (32)$$

and s_1 and s_2 are now given by

$$s_1 = \frac{\ln\left(\frac{S}{K}\right) + \left(r + \frac{\rho\mu}{\xi}\right)\tau + \left(-\rho^2 - \frac{\rho\xi}{2} + \frac{1}{2}\right)\omega + \frac{\rho}{\xi}\ln\left(\frac{V_i}{V_f}\right)}{\sqrt{(1 - \rho^2)\omega}} \quad (33)$$

$$s_2 = s_1 - \sqrt{(1 - \rho^2)\omega} \quad (34)$$

For the case considered in Baaquie [1], we have $\lambda = 0$ and $\alpha = 1$. In this case, we have $\eta = \zeta = \int_0^\tau e^{y/2} dt$ which gives us

$$f(x, y, t) = \left\langle SN(s_1) \exp\left(-\frac{\rho^2\omega}{2} - \frac{2\rho}{\xi}\left(V_i^{1/2} - V_f^{1/2}\right) - \frac{\rho}{\xi}\left(\mu - \frac{\xi^2}{2}\right)\eta\right) - Ke^{-r\tau}N(s_2) \right\rangle \quad (35)$$

where s_1 and s_2 are now given by

$$s_1 = \frac{\ln\left(\frac{S}{K}\right) + r\tau + \left(-\rho^2 + \frac{1}{2}\right)\omega + \frac{2\rho}{\xi}\left(V_i^{1/2} - V_f^{1/2}\right) + \frac{\rho}{\xi}\left(\mu - \frac{\xi^2}{2}\right)\eta}{\sqrt{(1 - \rho^2)\omega}} \quad (36)$$

$$s_2 = s_1 - \sqrt{(1 - \rho^2)\omega} \quad (37)$$

which is somewhat more complicated since two functionals, ω and η of the volatility path are involved. In this case, however, a perturbation analysis can be used to derive an approximate form for the probability distribution functions of the functionals. Due to this fortunate occurrence, a series solution to this problem can be obtained.

The probability density function (pdf) for the functionals is a very difficult quantity to obtain. The probability density function for $\int_0^\tau V dt$ was obtained for the special case $\alpha = 1/2$ in Stein and Stein [?]⁴. Stein and Stein [?] have used this probability distribution function and the “straightforward” solution for $\rho = 0$ to get an analytic form of the solution for this case. We now see that the result can be extended to non-zero ρ if we can find the joint probability density function of this functional and $V_i - V_f$. While the individual probability distribution functions can be obtained (the pdf for ω is obtained in Stein [?] and the pdf for $V_i - V_f$ is trivial), they are not independent.

2.5 Risk-Neutrality

We show that the expected value of the underlying security S whose initial value is S_0 is given by $S_0 e^{rt}$ after time t has elapsed for a large class of stochastic processes including the one we are considering in this thesis. In other words, we show that $A = e^{-rt} S$ is a martingale.

We first change variables from S to A in (5) (changing ϕ to r in accordance with risk-neutral valuation) to obtain

$$dA = Ae^{y/2} dz_1 \quad (38)$$

(where z_1 is the time integral of W and hence a Wiener process) where y may depend on A (y can be stochastic). We now consider the more general process

$$dA = f(A, y) dz_1 \quad (39)$$

⁴The original solution for simple Brownian motion was obtained way back in 1944 by Cameron and Martin [7]

We note that $E[dA] = 0$ so that $E[A(t+dt)|A(t) = A_0] = A_0$. In other words, we see that A is a martingale. Hence, we have shown the result. In general, a martingale process cannot have a drift term.

While the result is simple, it has important consequences. We note that risk-neutrality alone cannot determine any constraints for the volatility process. Any volatility process whatsoever satisfies risk-neutrality.

3 Numerical Algorithm

3.1 A Short, Quick Reminder of the Monte Carlo Method

The Monte Carlo algorithm to integrate

$$\int_A f(X)dX \tag{40}$$

where X can be (and, in fact, usually is) a multi-dimensional variable and A is a subset of the domain of X requires us to split $f(X) = g(X)p(X)$ so that $\int_A p(X)dX = 1$ (in other words, so that $p(X)$ is a valid probability density function). The algorithm then states that an estimate for the integral is given by $\langle g(X_i) \rangle = \frac{1}{N} \sum_{i=1}^N g(X_i)$ where the configurations X_i are generated randomly according to the probability density function $p(X)$.

The error of the Monte Carlo method goes as $\frac{1}{\sqrt{N}}$ as a consequence of the central limit theorem as long as there is no correlation between the configurations produced. (Though in general this condition is difficult to satisfy, we shall see later that we can easily satisfy it for this case). While this error may not look very impressive, it is often the best that can be managed for X which have a large number of dimensions. For the present problem, we have a very large number of dimensions (in fact the exact problem has an infinite number of dimensions) and the Monte-Carlo method is the most practical one available for it.

3.2 A Monte Carlo Method for this Problem

The Monte Carlo based numerical approaches of Hull and White [14,16], Finucane [12] and Mills [25] are all generalized forms of the Binomial tree in which for discrete time $t_n = n\frac{\tau}{N}$, the stock price x_n and volatility y_n are considered as random variables and both of which are updated. For the case of N -steps, we need to update N^2 variables for obtaining a new configuration. In eq(90), we have a drastic simplification since the path integral over the x_i

variables for the general case of $\rho \neq 0$ has been evaluated *exactly* by analytical means. Hence in basing numerical simulation on eq(90), one needs to generate new configurations for only the y_n random variables, namely N variables, reducing the computational time required by a factor of N .

For this problem, we choose the following probability density function

$$p(Y) = \left(\prod_{i=1}^{N-1} \frac{e^{y_i(1-\alpha)}}{\sqrt{2\pi\epsilon\xi}} \right) e^{S_0} \quad (41)$$

where Y is the set of variables y_i (and is hence N -dimensional) and S_0 is given in (93). Hence, we see that

$$g(Y) = \frac{e^{S_1}}{\sqrt{2\pi\epsilon(1-\rho^2) \sum_{i=1}^N e^{y_i}}} \quad (42)$$

where S_1 is given in (83) since the integral we are performing is

$$\int DY \left(\prod_{i=1}^{N-1} e^{y_i(1-\alpha)} \right) \frac{e^{S_0+S_1}}{\sqrt{2\pi\epsilon(1-\rho^2) \sum_{i=1}^N e^{y_i}}} \quad (43)$$

where

$$DY = dy_0 \prod_{i=1}^{N-1} \frac{dy_i}{\xi\sqrt{2\pi\epsilon}}$$

We now have to produce configurations Y with the probability distribution $p(Y)$. While $p(Y)$ looks rather complicated, it has a simple interpretation. It is the probability distribution for a discretized random walk performed by y . To see this, let us first use Ito's lemma to find the process followed by y . We find, from eq(proc2) and eq(variable),

$$dy = \left(\lambda e^{-y} + \mu - \frac{\xi^2 e^{2y(\alpha-1)}}{2} \right) dt + \xi e^{y(\alpha-1)} Q dt \quad (44)$$

We can now discretize the process using Euler's method to obtain

$$\delta y_i = \left(\lambda e^{-y_i} + \mu - \frac{\xi^2 e^{2y_i(\alpha-1)}}{2} \right) \epsilon + \xi e^{y_i(\alpha-1)} Z \sqrt{\epsilon} \quad (45)$$

where $\delta y_i = y_i - y_{i-1}$, ϵ is the time step and Z is a standard normal variable. Since we are using $\tau = T - t$ as the time variable, the time step is actually $-\epsilon$. Hence, δy_i is a normal

random variable with mean $(-\lambda e^{-y_i} - \mu + \xi^2 e^{2y_i(\alpha-1)}/2) \epsilon$ and variance $\xi^2 e^{2y_i(\alpha-1)} \epsilon$ and the probability density function is given by

$$f_i = \frac{e^{y_i(1-\alpha)}}{\xi \sqrt{2\pi\epsilon}} \exp \left(-\frac{\epsilon e^{2y_i(1-\alpha)}}{2\xi^2} \left(\frac{\delta y_i}{\epsilon} + \lambda e^{-y_i} + \mu - \frac{\xi^2 e^{2y_i(\alpha-1)}}{2} \right)^2 \right) \quad (46)$$

Hence, the joint probability density function for the discretized process is given by

$$f = \prod_{i=1}^{N-1} f_i = \left(\prod_{i=1}^{N-1} \frac{e^{y_i(1-\alpha)}}{\sqrt{2\pi\epsilon\xi}} \right) e^{S_0} \quad (47)$$

which is the same as (41).

In this simulation, we will use Euler's method to find the volatility paths since these paths are generated with the requisite probability distribution.

The algorithm to find a Monte Carlo estimate of the propagator $p = \langle x, y | e^{-\hat{H}\tau} | x' \rangle$ is as follows

1. $p := 0$ (Initialization)
2. For $i := 1$ to N
3. Generate a path Y for y using (44)
4. $p := p + g(Y)/N$ (where $g(Y)$ is defined in (42))
5. End For

The paths must be generated backwards starting from y_N which is the initial value of $\ln V$ to obtain all the y_0 . Since the equations are time symmetric (after, of course, reversing the drift terms), this presents no problem. This will have to be repeated for all the x' that we wish to integrate over. However, during implementation it is found to be more advantageous to generate the paths only once, storing the important terms $t = N\epsilon$, $t_1 = \sum_{i=1}^N e^{y_i}$ and

$$t_2 = \frac{\rho}{\epsilon} \sum_{i=1}^N e^{y_i(3/2-\alpha)} \left(\frac{\delta y_i}{\epsilon} + \lambda e^{-y_i} + \mu - \frac{\xi^2 e^{2y_i(\alpha-1)}}{2} \right)$$

which are sufficient to determine S_1 once x' is given ($S_1 = -\frac{1}{2\epsilon(1-\rho^2)t_1} (x - x' + (r - q)t - \epsilon (\frac{t_1}{2} + t_2))^2$) where q is the annualized dividend. That S_1 can be computed using this limited information is fortunate as storing all the paths explicitly would require a very large memory (10MB for 10,000 configurations as compared to 160kB when storing only the essential combinations of

terms). The alternative of generating paths for each value of x' (as in the naïve algorithm above) is unacceptable due to the very large run time required using this approach.

The propagator must finally be integrated over the final wave function to obtain the option price. The accuracy of this numerical quadrature depends on the spacing h between successive values of x' . This means that we have to find the propagator for several values of x' to obtain reasonable accuracy which is computationally very expensive. We found it better to find the propagator using the above Monte Carlo method for only about 100 equally spaced values of x' over the range of the quadrature and using cubic splines to interpolate it at the other quadrature points. This produces excellent results (as we shall see later) as the propagator seems to be an extremely smooth function of x' .

Hence, the revised algorithm is of the form

1. For $i := 1$ to N
2. Generate a path Y for y using (44)
3. Store t_1 and t_2 for the path
4. End For
5. For $x' :=$ beginning of range to end of range
6. Find the Monte Carlo estimate for the propagator at large intervals of x' using t_1 and t_2 from the paths.
7. End For
8. For $x' :=$ beginning of range to end of range
9. Find the propagator at small intervals of x' using cubic spline interpolation over the values of the propagator found previously and integrate over the final wave function (payoff)
10. End For
11. Return option price

The numerical quadrature was performed using Simpson's rule. While Simpson's rule is a relatively low order method, it was deemed sufficient as the error in quadrature is negligible

compared to the Monte Carlo error in the propagator. For the special case of the European call option, it is possible to integrate analytically over the splines as the payoff is piecewise linear. However, this was not done as firstly, the error in the quadrature was negligible compared to the Monte Carlo error and secondly (and more importantly) we wanted to make the program general so that it is able to price any derivative based on the underlying security which has only one payoff date.

For the special case of functions which can be expressed as piecewise polynomial functions, the integration can be carried out analytically and we can then just generate the paths and find the expectation over the generalized Black-Scholes prices. While this method has the advantages of being elegant, easy to program and completely eliminating the error due to the integration, it has the disadvantage that we have to carry out the integration first before we can write the program which will be specific to the given payoff. We have implemented this approach for call options but found no significant improvement in run time (it runs about 1% faster).

The above algorithm may appear unstable in the limit $\epsilon \rightarrow 0$ since in this case $\frac{\delta y}{\epsilon} = O\left(\sqrt{\frac{1}{\epsilon}}\right)$. Fortunately, in the case of our simulations this is not a problem as our step size was always large enough to avoid this problem. If this is a problem in any simulation, this can be easily handled as the propagator can always be written as a functional of the paths as given in (25). We can then generate paths for V or y using (6), store the functionals (we will now need 5 terms $t_1 = \omega$ (which is the same as above), $t_2 = \theta = \sum_{i=1}^N e^{y_i(1/2-\alpha)}$, $t_3 = \eta = \sum_{i=1}^N e^{y_i(3/2-\alpha)}$, $t_4 = \zeta = \sum_{i=1}^N e^{y_i(\alpha-1/2)}$ and $t_5 = e^{y_0(3/2-\alpha)}$). We can then proceed to find the propagator as above (of course, now writing S_1 as a function of t_i , $i = 1, \dots, 5$) and integrate over the final payoff. For the special case of the European call option, one can make this method slightly more efficient by averaging over the generalized Black-Scholes prices (26). We did not use this method since it takes longer to compute the propagator using five terms and because the memory requirements are higher.

4 Numerical Results for the General Case

We performed simulations on 90 day options setting an initial volatility of 25% per annum which is a figure comparable to the historical data. We performed simulations for $\alpha = 0, \frac{1}{2}, \frac{3}{4}$ and 1 with correlations ranging from -0.5 to 0.5 in steps of 0.1. We set $\lambda = \mu = 0$ for most of the simulations. Some simulations with mean-reverting volatility processes were performed

for the purposes of investigating the effect of mean-reversion on option prices.

The following parameters have the following values unless otherwise stated : $S_0 = 100$, $r = 5\%$, $q = 0\%$, $t = 90$ days, $\lambda = 0$ and $\mu = 0$. Most of the simulations have been performed using 128 time steps and 500,000 Monte Carlo configurations. The exceptions have been for $\alpha = \frac{1}{2}$ where we have used 512 time steps and the simulations we have performed for the other values of α to check that the number of time steps is sufficient. The error bars in all the graphs refer to the standard error obtained from the Monte Carlo simulation.

4.1 The Effect of ρ on Option Prices

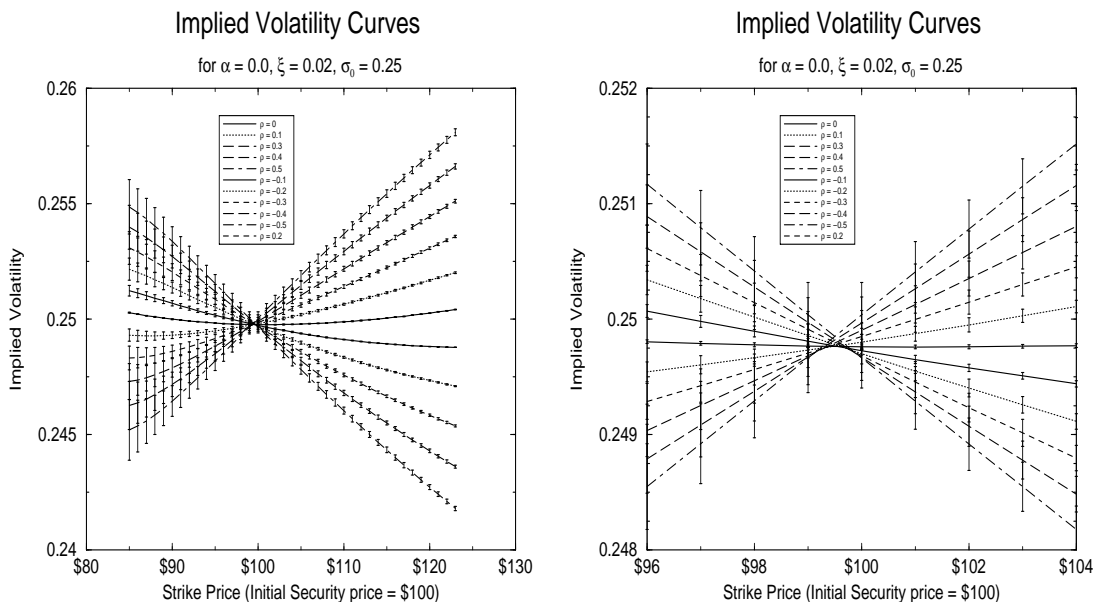


Figure 1: Implied volatility curves showing the effect of ρ on option prices when $\alpha = 0$. We can see that positive ρ leads to an increase in the option price when the strike price is high and a decrease when the strike price is low while negative ρ has the opposite effect.

The correlation ρ has a very large impact on the implied volatility curve irrespective of the values of the other parameters. When $\rho = 0$, we see that the implied volatility is in the form of a smile with the minimum near the present value of the underlying security (S_0). As ρ increases, we find that the implied volatility increases for large strike prices and decreases for small strike prices. This can be easily seen in the graphs in figures 1, 2, 3 and 4. We can also see that the deviation of the implied volatility from the initial volatility is much higher when the correlation is non-zero. These results are consistent with those reported in Hull

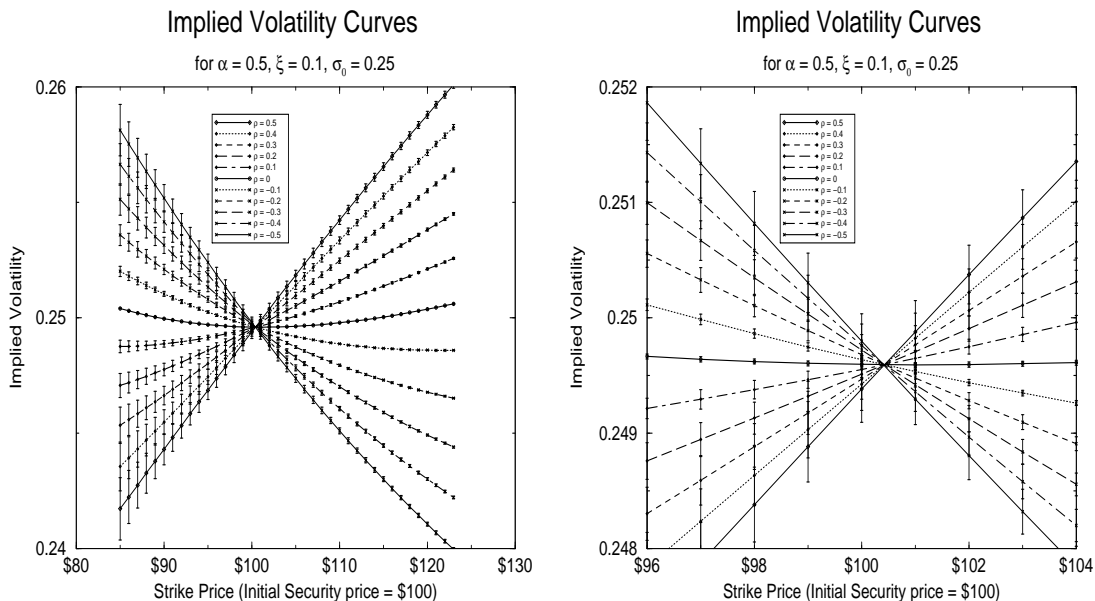


Figure 2: Implied volatility curves showing the effect of ρ on option prices when $\alpha = \frac{1}{2}$. We can see that positive ρ leads to an increase in the option price when the strike price is high and a decrease when the strike price is low while negative ρ has the opposite effect.

and White [15], Heston [13], Johnson and Shanno [18] and Scott [30].

This can be explained in terms of the propagator obtained by the Monte Carlo simulation. From figure 5, we see that the propagator for positive correlation is greater for very large $x' - x$ (where $x = \ln S_0$ and $x' = \ln S$) as compared to the propagator for zero correlation. This essentially means that the probability for the underlying security price reaching very large values is higher when the correlation is positive. Hence, the price of options with a very large strike price is larger when the correlation between the processes for the underlying security price and the volatility process is positive. For negative correlation, we see that the propagator for small, positive $x' - x$ is greater than that for zero or positive correlation. Hence, for options whose strike price is smaller, there are two competing factors, the propagator for x' slightly larger than x and the propagator when $x' \gg x$. For relatively large strike prices, the latter is more important and the implied volatility is higher when the correlation is positive while for relatively small strike prices, the former is more important and the price when the correlation is positive is lesser than for zero or negative correlation. The same analysis can be performed for the case of negative correlation and is consistent with the simulated results.

We can also intuitively examine why the propagator has this form when the two processes are correlated. If the two processes are positively correlated, we have two possibilities. If the price initially increases, so will the volatility and hence, large price increases become more likely while small price increases become less likely. On the other hand, if the price initially decreases, so will the volatility and the price is more likely to remain at that value. Hence, for positive correlation, the propagator must be higher for prices slightly lower and much greater than the initial price and lower for prices slightly larger than the initial price. The reverse holds true for negative correlation. This naive reasoning is fully borne out in figure 5.

We were unable to simulate frowns or any sort of kinks in the implied volatility curve for any values of the parameters. This seems to suggest that stochastic volatility even with arbitrary correlation places some constraints on the shape of the implied volatility curve. We can use this to check whether the hypothesis that the volatility is stochastic is reasonable or otherwise. We note that the empirical implied volatility curve used for our calibration does satisfy this criterion.

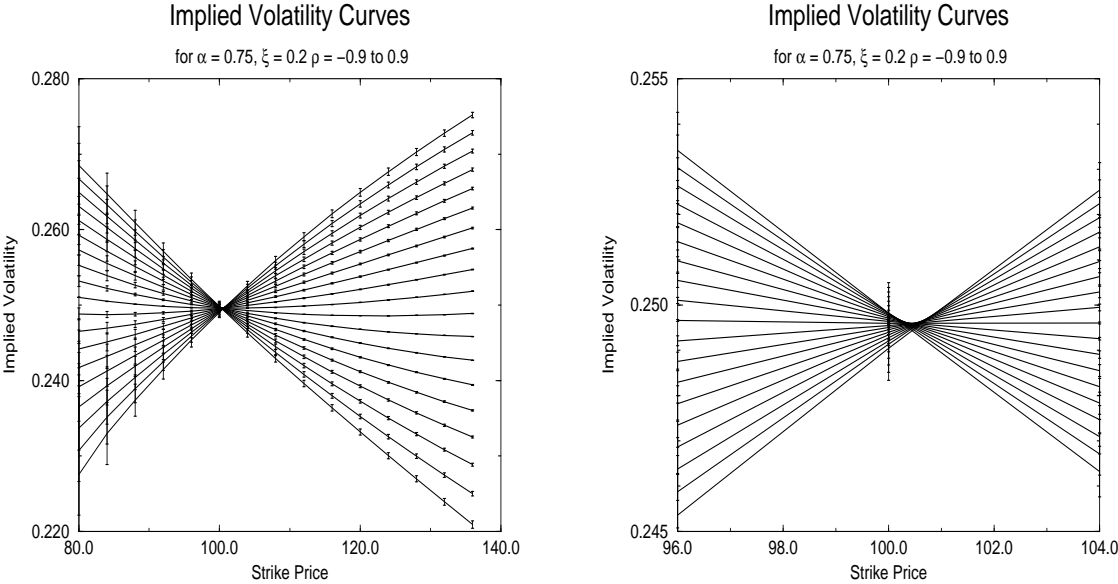


Figure 3: Implied volatility curves showing the effect of ρ on option prices for $\alpha = 1$. We can see that positive ρ leads to an increase in the option price when the strike price is high and a decrease when the strike price is low while negative ρ has the opposite effect.

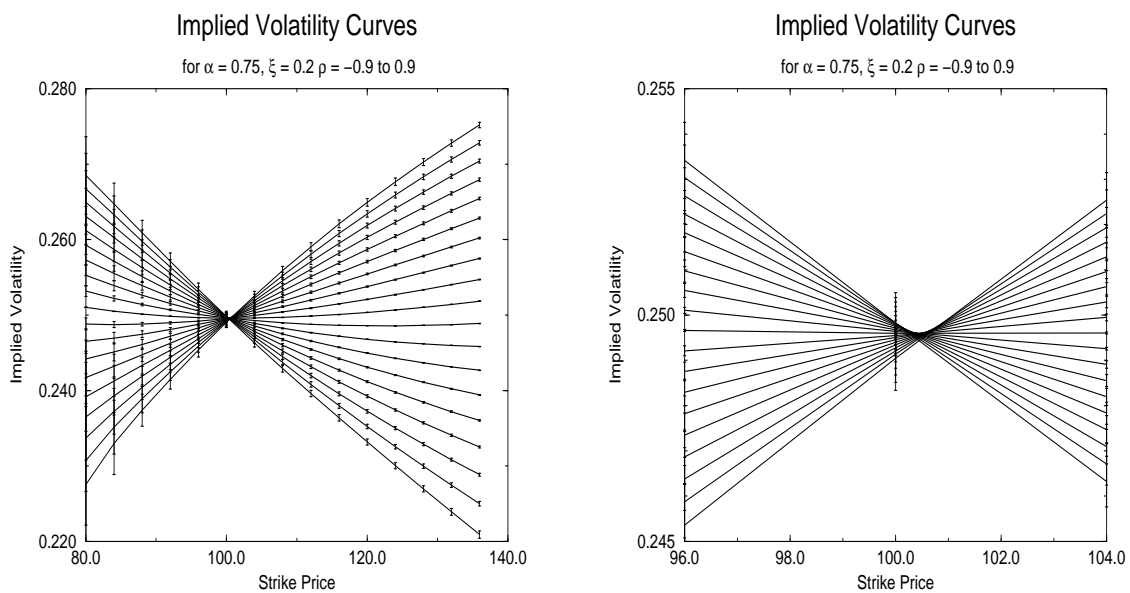


Figure 4: Implied volatility curves showing the effect of ρ on option prices for $\alpha = 1$. The curves for the different values of ρ are in ascending order according to the slope (in other words, the slope increases monotonically with ρ). Hence, we can see that positive ρ leads to an increase in the option price when the strike price is high and a decrease when the strike price is low while negative ρ has the opposite effect.

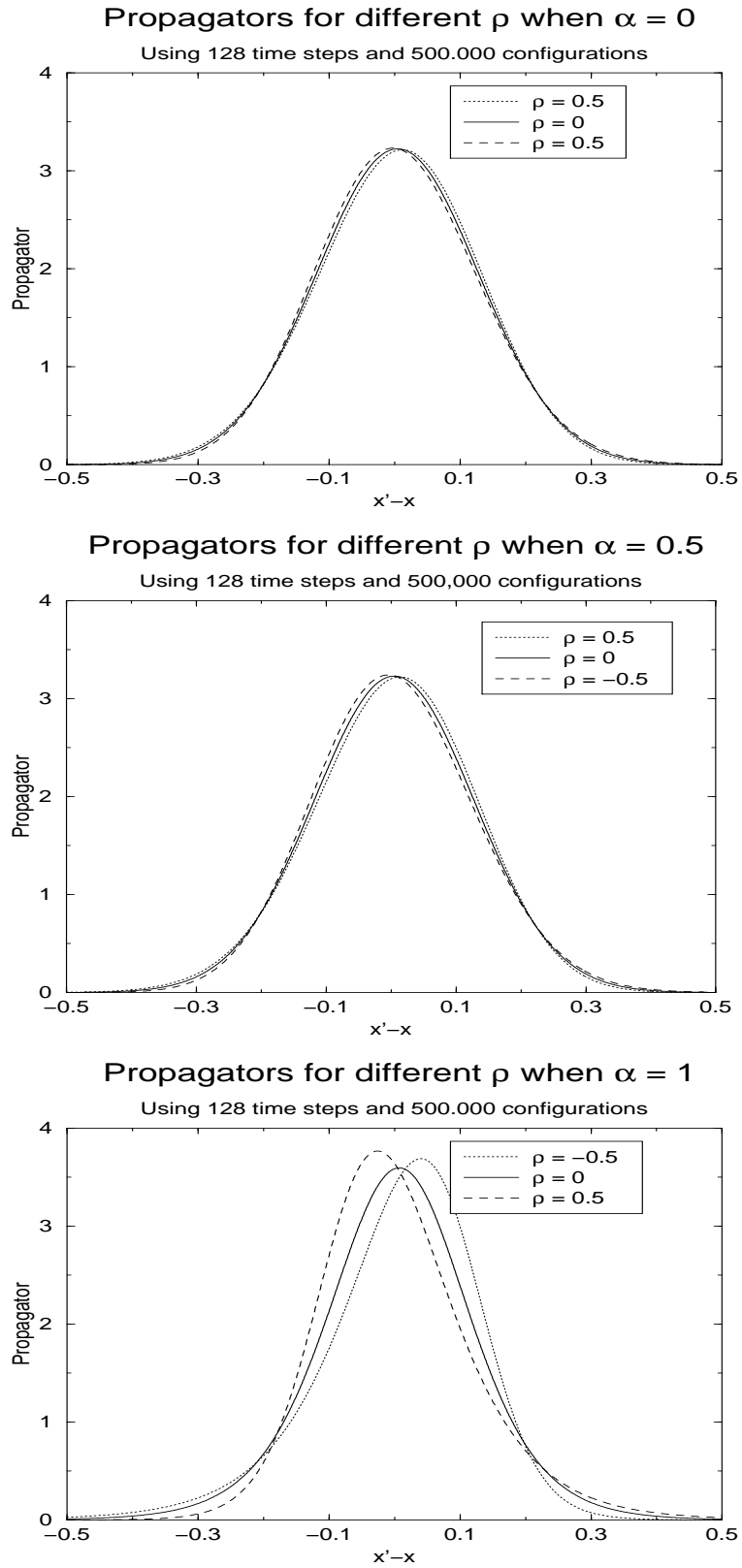


Figure 5: Propagators for different ρ when $\alpha = 0, 0.5$ and 1 .

4.2 The Effect of Mean Reversion on the Option Price

Several authors including Heston [13] and Hull and White [15] have considered mean-reverting processes as there is some empirical evidence that the volatility follows a mean-reverting process. We note that our process also includes mean reversion since λ and μ can be adjusted so that the volatility performs a mean-reverted process. We find that the effect of mean reversion is straightforward in that it only seems to change the implied volatility curve so that it moves closer to the mean value.

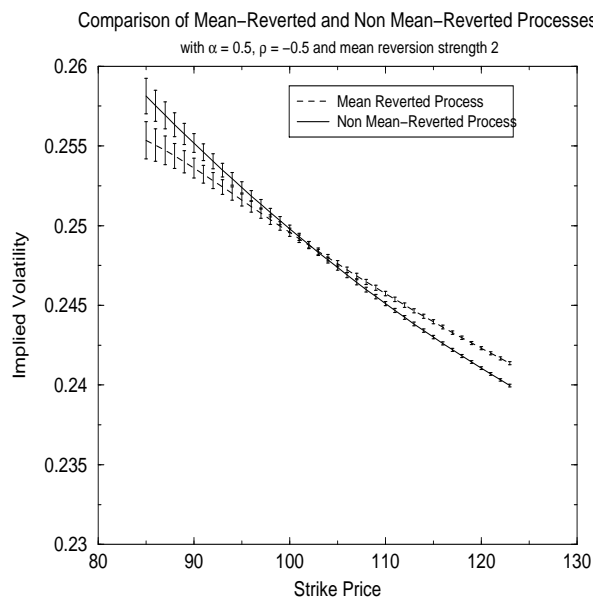


Figure 6: Comparison of a mean-reverting process and a non mean-reverting process

For example, consider figure 6. In this case, we used an initial volatility of $V_0 = 0.0625$ (so that $\sigma_0 = 0.25$). We set $\lambda = 0.125 = 2 \times 0.0625$ and $\mu = -2$ so that the volatility is performing a mean-reverting process with the mean the same as the initial value. We see that we indeed obtain the expected behaviour as compared to the non mean-reverting process. The mean reverting process just produces an implied volatility curve of a similar shape which is closer to the mean value.

4.3 Calibration with Market Data

We compare our model with market data to see how well it works. Since volatility information is available only as 10 day or 50 day averages and the options we were comparing the market

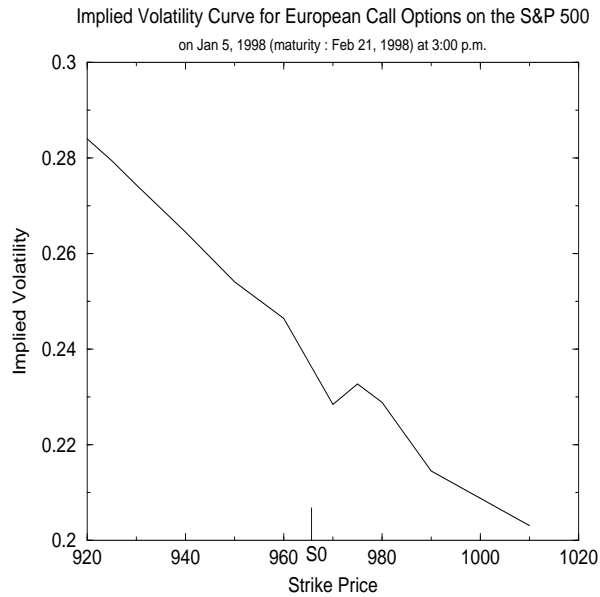


Figure 7: The implied volatility curve for European call options on the S&P 500 Index maturing on Feb. 21, 1998 on Jan. 5, 1998 at 3 p.m.

data to had 47 days to expiration, we used the initial volatility as a free parameter. The market data used were the prices of European call option on the Standard and Poor's 500 Index at 3 p.m. on Jan 5, 1998 with the maturity date given as Feb 21, 1998. The prices taken were either the trade nearest to 3 p.m. if it was within half an hour and the average of the bid and ask prices closest to 3 p.m. otherwise. The data are presented in table 1. We note that the number of option prices we have is much larger than the number of free parameters in the model. The value of the Standard and Poor's 500 Index at the same time was given as 965.61 (since the S&P 500 is traded several times every minute on the average, obtaining data for it presented no problem). The risk-free interest rate r was 5.131% and the annualized dividend yield was 1.617% at the same time. The implied volatility curve for the market data is shown in figure 7.

Looking at the market data, we immediately see that the implied volatility is almost monotonically declining. Hence, according to our model, the correlation is very probably negative. We also see that the implied volatilities vary within quite a wide range implying that ξ must be quite high as the volatility must vary widely for the implied volatility to do so. Further, the value of the initial volatility can be seen to be about 25% (according to our model, not the actual initial volatility which we could not determine with reasonable

Strike Price	Option Price
920	68.0
925	64.125
930	60.25
940	52.75
950	45.5
960	39.0
970	31.5
975	29.75
980	27.0
990	21.0
1010	13.0

Table 1: The prices of European call options on the S&P 500 Index whose maturity was on 21 Feb, 1998 on Jan 5, 1998 at 3:00 p.m. The prices were taken to be those of the closest trade if there was a trade within half an hour and the average of the bid and ask prices otherwise.

accuracy).

Since there is no simple functional form for the option price, the calibration was performed manually. The reasoning above enabled us to start with fairly accurate values. Thus, while we cannot guarantee that the result is the best fit curve in any precise sense, we can see from figure 8 that the fit is very good. While the in the money options seem to not fit so well, this might be because these options are thinly traded.

The skeptical reader might comment that the number of free parameters (4) is quite large and that a fairly wide range of empirical curves might be fitted. However, we note that our model predicts only three possibilities for the implied volatility curve, namely a “smile” (low correlation), monotonically increasing (positive correlation) or monotonically decreasing⁵ (negative correlation). The existence of a “frown” or kinks in the implied volatility curve would be disastrous for the model. (There does appear to be a small kink in the empirical

⁵The simulations for non-zero correlation show more interesting behaviour but we are interested only in the behaviour for strike prices close to the underlying security price as these are the only kind of options traded in the market

curve but the scale of the kink is very small and occurs for only one value.)

Indeed, as shown in figure 8, some calibrated values of the parameters for European call options on the S&P 500 Index on 21 Feb. 1998 are $\sigma = 0.27$, $\rho = -0.99$, $\xi = 3.7$ and $\alpha = 1$.

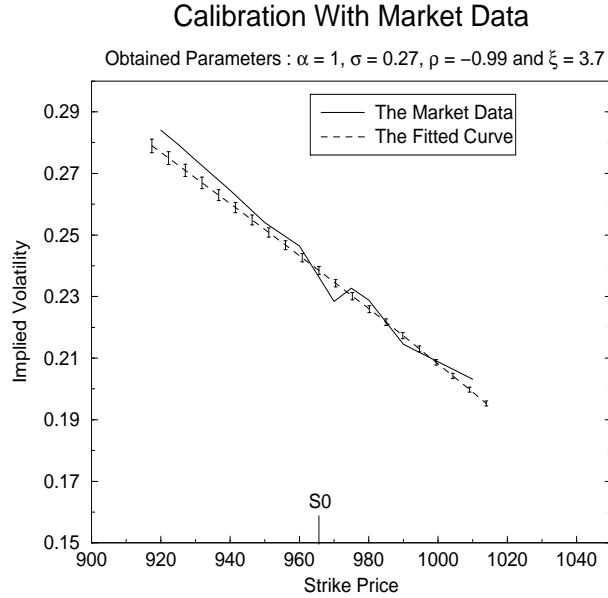


Figure 8: The above graph shows the implied volatility curve produced by the fitted values together with the market data.

5 Numerical Algorithm for $\alpha = 1$

In our previous simulation, we found that the value of α for many typical market data is approximately one, that is $\alpha \approx 1$. It turns out that for this case we have very efficient algorithms, namely the bisection method. This algorithm is of intrinsic interest and allows us to examine the behavior of stochastic volatility in great detail. In particular, we investigate the effect of ρ on implied volatility and show how smiles turn to frowns and so forth. We have intentionally chosen the maturity time to be one year so as to magnify the effects. To consider the numerical simulation of our model for $\alpha = 1$ and $\lambda = 0$, we first set $\alpha = 1$ in eq(90) to eq(93) to get

$$\langle x, y | e^{-\tau H} | x' \rangle = \int DY \frac{e^{S_0 + S_1}}{\sqrt{2\pi\epsilon(1 - \rho^2) \sum_{i=1}^N e^{y_i}}} \quad (48)$$

where

$$S_0 = -\frac{\epsilon}{2\xi^2} \sum_{i=1}^N \left(\frac{\delta y_i}{\epsilon} + \mu - \frac{\xi^2}{2} \right)^2 \quad (49a)$$

$$S_1 = -\frac{1}{2(1-\rho^2)\epsilon \sum_{i=1}^N e^{y_i}} \left\{ x - x' + \epsilon \sum_{i=1}^N \left(r - \frac{1}{2} e^{y_i} \right) - \frac{\rho}{\xi} \sum_{i=1}^N e^{\frac{y_i}{2}} \left[\delta y_i + \epsilon \left(\mu - \frac{\xi^2}{2} \right) \right] \right\}^2 \quad (49b)$$

$$\delta y_i = y_i - y_{i-1}, \quad y_N = y = \text{initial volatility.} \quad (49c)$$

In eq(48), we have used the notation $\int DY$ to mean product $dy_0 \left(\prod_{i=1}^{N-1} \int_{-\infty}^{\infty} \frac{dy_i}{\sqrt{2\pi\epsilon\xi^2}} \right)$.

Moreover, the complete information regarding the dynamics and evolution of stock price $S(t)$ and its volatility $V(t)$, their cross correlators as well as the fluctuations is given by the discrete time path integral equation

$$\begin{aligned} \langle x, y | e^{-\tau H} | x' \rangle &= \int_{-\infty}^{\infty} dy' p(x, y, \tau | x', y') \\ &= \lim_{N \rightarrow \infty} \int DX DY e^{S'} \end{aligned} \quad (50)$$

where, for $\epsilon = \frac{\tau}{N}$,

$$\int DX = \frac{e^{-\frac{y_N}{2}}}{\sqrt{2\pi\epsilon(1-\rho^2)}} \prod_{i=1}^{N-1} \int_{-\infty}^{\infty} \frac{dx_i e^{-\frac{y_i}{2}}}{\sqrt{2\pi\epsilon(1-\rho^2)}}$$

and where the ‘action’ S' is defined by

$$\begin{aligned} S' &= -\frac{1}{2}\epsilon \sum_{i=1}^N \left\{ \frac{1}{\xi^2} \left(\frac{\delta y_i}{\epsilon} + \mu - \frac{1}{2}\xi^2 \right)^2 \right. \\ &\quad \left. + \frac{e^{-y_i}}{(1-\rho^2)} \left[\frac{\delta x_i}{\epsilon} + r - \frac{1}{2}e^{y_i} - \frac{\rho}{\xi} e^{\frac{y_i}{2}} \left(\frac{\delta y_i}{\epsilon} + \mu - \frac{1}{2}\xi^2 \right) \right]^2 + O(\epsilon) \right\} \end{aligned} \quad (51)$$

To determine numerically the probability $P(x, y, \tau | x', y')$, one could use the Metropolis method [3] to evaluate numerically the path integral given in eq(48) by finding the expectation value of $\frac{e^{S_1}}{\sqrt{2\pi\epsilon(1-\rho^2) \sum_{i=1}^N e^{y_i}}}$, the functional average being performed over configurations of y_n with a probability distribution given by e^{S_0} , where S_0 and S_1 are given by the formulae in eq(49a) and eq(49b) respectively. However, given the special form of S_0 which can be interpreted as the kinetic energy of a free quantum particle, a more efficient method

is to generate configurations based on the bisection method [27]. In the bisection method, unlike the Metropolis case, all configurations generated are accepted and this is therefore a better algorithm.

In the bisection method, the interval τ is first divided into half; the sample value of y at the center is generated by $y(\frac{\tau}{2}) = \frac{1}{2}\{y(0) + y(\tau) + \tau^{1/2}z\}$, where z is a standard normal variate, $N(0, 1)$, namely a normal random variable with mean zero and variance of unity. The sub-intervals $[0, \tau/2]$ and $[\tau/2, \tau]$ are further bisected and the above algorithm is repeated and so forth. In general, the interval $[a, b]$ is bisected and the sample value at the mid-point is given by $y(\frac{a+b}{2}) = \frac{1}{2}\{y(a) + y(b) + (b-a)^{1/2}z\}$, where $y(a)$ and $y(b)$ are the values of $y(t)$ at the points a and b respectively. After N bisections, we obtain a time lattice with 2^N discrete points with spacing $\epsilon = \frac{\tau}{2^N}$; and the average of $\frac{e^{S_1}}{\sqrt{2\pi\epsilon(1-\rho^2)\sum_{i=1}^N e^{y_i}}}$ is taken over the configurations generated.

5.1 Pseudo-Codes for the Algorithm

Essentially, the main formula that we used to simulate the derivative pricing is eq(48). To compute the derivative prices, the program in our simulation can be broken into three major steps:

- Generate 2^N y_i variables using the bisection method,
- Evaluate the path integration using eq(48),
- Compute the derivative price.

The first step in the computation requires the generation of 2^N variables using the bisection method. The pseudo-code for the bisection subroutine is as follows:

- Initialize an array of size $2^N + 1$ (Call it Rand Y(i), for random y_i)
- Set y_1 and y_M where $M = 2^N + 1$ to the initial and end values of the volatility.
- Do J=1 to m
- Do I=1 to 2^{J-1}
- Call Normal Variate $N(0, 1)$, Norm

- Rand Y($\frac{M(2^I - 1) + (2^J - 2^I + 1)}{2^J}$) $\leftarrow \frac{1}{2}\{$ Rand Y($\frac{M(I - 1) + (2^{J-1} - 1 + 1)}{2^{J-1}}$)
 $+ \text{Rand Y}(\frac{IM + (2^{J-1} - 1)}{2^{J-1}}) + \text{Norm}(\sqrt{\frac{\tau}{2^{J-1}}})\}$
- End of I Loop.
- End of J Loop.

Computation of the path integration using eq(48) is straightforward. We first fix x and y to be some initial value of stock price and volatility. We then divide the variable x' into N divisions⁶ and store them as arrays. For each value of x' and y' , one then calls the subroutine Bisect which essentially provides a normalized array of $2^M + 1$ points and computes using eq(49b), the average of $\frac{e^{S_1}}{\sqrt{2\pi\epsilon(1 - \rho^2) \sum_{i=1}^N e^{y_i}}}$. This procedure effectively yields the probability in eq(48). As a final step, one computes the simulated derivative pricing by integrating over y' using a simple integration algorithm based on Bode's rule. This integration is exact for any polynomial up to and including degree 5.

6 Results of Numerical Simulations for $\alpha = 1$ and $\lambda = 0$

6.1 Parameters

There are a number of parameters which we can fix freely without affecting the analysis of the behaviors in the implied volatility curves. Based on the current market data, we have set the interest rate arbitrarily at a plausible rate of 6 % per annum throughout the simulation. The other free parameters, which are fixed throughout the simulations, assume the following values:

Interest Rate, r :	0.06 or 6 %
Time interval, τ :	1 year
Number of bisections:	32
Number of points for x' integration:	100
Initial Volatility, V :	1 (i.e. $y_N = 0$)

⁶Typically, due to the exponential relation of the variables with the stock price, a range between ± 7 should be sufficient.

6.2 Simulations

Under the path integral formalism, one can vary the new parameters like ρ , ξ and μ in the model and study its effect on the option price. With sufficient simulation, one hopes to identify precisely the nature of these changes and interpret their importance to the fluctuation of the option prices in the market. Like Black-Scholes model, one can also get closed form expressions of the option prices under certain constraints and limits. Unlike Black-Scholes model, it does not assume constant volatility and thus provides greater flexibility for a calibration of the market data.

We shall see that the variation of the call option prices against strike prices for different values of correlation parameter, ρ can differ significantly from Black-Scholes case. We simulate option prices with stochastic volatility using a stock price of 100. In figure 9, we have plotted the two graphs of call option prices against strike price for a fixed $\rho = 0.001$ but differing values of ξ . In this simulation, we have set $\mu = 0$. In one graph, we have kept ξ as 0.01 while in the other graph we have fixed the same parameter as 0.001.

graphic1.gif

Figure 9: Graph of the call option price with stochastic volatility against strike prices for $\mu = 0$ and $\rho = 0.001$ is plotted. A similar graph computed from Black-Scholes equation is also drawn for comparison.

A graph of the option prices computed from Black-Scholes model with a variance of unity is also provided. We observe that despite the small value of $\rho = 0.001$, there are still some drastic differences between the option prices simulated with stochastic volatility and the standard Black-Scholes equation. The difference seems drastic for strike prices below the at-the-money position of 100 units but for strike prices above the at-the-money position, this difference may not be large. We have checked numerically that the option price with stochastic volatility converges, as expected, to that predicted by the Black-Scholes formula in the limit $\xi \rightarrow 0$.

We simulate and calculate the implied volatilities for various values of ρ holding stock price constant at 100 and then allowing the strike prices to vary. Our initial simulation are based on values of ρ between 0.1 and 0.9. We believe that one can glean important information on the *behaviour* of the curves with these values. The values of μ and ξ have again been arbitrarily fixed at 0.1. The simulated data for $\rho = 0.1$ to $\rho = 0.3$ is tabulated

and shown in table 2. The implied volatility curves for $\rho = 0.1, 0.2, 0.3$ are plotted against different strike prices in figure 10. The graphs clearly show that the volatility curves assume frowns for these positive values of ρ .

graphic2.gif

Figure 10: Graphs of implied volatility curves for positive ρ values between 0.1 and 0.3. The parameters ξ and μ are set to 0.1 and the stock price is fixed at 100. These curves appear as ‘frowns’.

μ	0.1		0		0	
	$\rho = 0.1, \xi = 0.1$		$\rho = 0.01, \xi = 0.01$		$\rho = -0.01, \xi = 0.01$	
Strike Price	Option	Volatility	Option	Volatility	Option	Volatility
75	31.2748	0.635	38.897	0.3216	76.615	2.16
80	30.6564	0.702	38.216	0.443	74.989	2.119
85	30.0967	0.749	37.351	0.5212	73.386	2.08
90	29.5342	0.79	36.584	0.5804	71.726	2.041
95	29.0275	0.827	35.907	0.6298	69.893	1.995
100	28.5038	0.861	35.318	0.6707	68.412	1.967
105	27.9804	0.888	34.648	0.7057	66.718	1.93
110	27.5226	0.911	33.992	0.7377	65.213	1.902
115	27.0136	0.931	33.283	0.7645	63.628	1.871
120	26.5956	0.95	32.666	0.7906	62.134	1.844
125	26.174	0.971	32.217	0.8138	60.737	1.821

Table 2: Simulated data values of call option prices and their implied volatilities for different strike prices with varying ρ values and for a stock price of 100

The parameter ρ measures the amount of correlation between the stock price and its volatility. Now, correlation coefficient can assume negative values and we should not disregard this possibility. Also, negative values of ρ tends to ‘whip’ up the value of the integrand in eq(49) or eq(51). We have seen from figure 10 that the volatility curves for positive ρ concave downwards as ‘frowns’. At this stage, we may be tempted to surmise that concavity and convexity of volatility curves are associated with positive and negative values of ρ respectively. We shall soon see that this is not true.

We investigate the volatility curves for negative ρ . For the case in which the stock price is fixed at 100 and the parameters $\mu = \xi$ are set to 0.1, the graphs of the implied volatilities against strike prices for $\rho = -0.1, -0.2, -0.3$ are given in figure 11. The volatility graph for $\rho = -0.1$ certainly concave upwards as ‘smiles’. However, the graphs for $\rho = -0.2$ and $\rho = -0.3$ flip over and appear as frowns again. Thus, negative values of ρ do not necessarily yield volatility curves which concave upwards as smiles.

graphic3.gif

Figure 11: Implied volatility curves for negative ρ values. The parameters μ and ξ are fixed at 0.1.

Under path integral formalism, it is always possible to expand the probability given in eq(48) perturbatively in powers of ξ when the values of ξ are in general very small ⁷ and evaluate exact closed-form expression for the coefficients in the expansion [16]. However, when ξ assumes typically the order of unity, ($\xi \sim 1$ which is what market data indicates) it is generally theoretically impossible to perform such an expansion and the perturbative method fails.

However, unlike perturbative analysis, the path integral formalism still permits numerical evaluation for these values of ξ . Some simulated results for large $\xi = 1$ with $\mu = 0.1$ are shown in figure 12. We also investigate the variation of the implied volatility curves against strike prices at different initial stock prices. When we fix the values of μ and ξ to 0.1. with $\rho = -0.1$, the volatility curves concave upwards as smiles for each stock price. In figure 13, we show our results for four different values of stock prices, namely 50, 75, 105 and 200. Note that the volatility curves for the last two stock prices, namely 105 and 150, appear to coincide with each other. We also note that the large value of μ which we have chosen for the model may have unnecessarily distorted the graphs in figure 13 and shifted them away from the at-the-money position.

graphic4.gif

Figure 12: Simulation of Implied Volatility curves for large values of $\xi(\xi = 1)$ in which perturbation analysis fails. The graphs in this figure are simulated $\mu = 0.1$ with varying ρ values.

⁷Strictly speaking, the values of the strike prices and stock prices must also be appropriately tuned before a perturbative approach is possible.

graphic5.gif

Figure 13: Graphs of implied volatility against strike price for varying values of stock price, S . In this simulation, the parameters μ , ξ and ρ have been arbitrarily fixed at 0.1, 0.1, -0.1

In most mature market, the value of ρ can be small for some securities. We simulate the volatility curves with μ set to zero and with the parameters ρ and ξ held small at -0.02 and 0.01 respectively. In this case, we note two interesting observations. Firstly, negative ρ values do not necessary lead to volatility curves which concave upwards as smiles. As seen in figure 15, the concavity of the volatility curves can vary with different stock prices. Secondly, if we plot the option prices generated in the simulation with a stock price of 100 and compare the graph with Black-Scholes model as in figure 14, we observe that the two graphs intersect near the strike price of 100. This result is consistent with the observations in some models [?] that stochastic volatility appear significant away from the at-the-money position. This means that implied volatility is lowest at-the-money and increases as the strike prices moves away from that position.

graphic6.gif

Figure 14: Graph of option price with μ , ξ and ρ set at 0, 0.01, -0.02 and the stock price fixed at 100 compared to the Black-Scholes model with the same initial volatility. We have also indicated the at-the-money position using a vertical line at the strike price of 100.

The initial volatility in our simulation has been fixed at 1 so that we can see the full effects of volatility to the option prices. Generally we would anticipate a smaller value of initial volatility for the market data. We have also performed simulations using a smaller initial volatility of 0.2. Figure 16 shows the different implied volatility curves which we have obtained using this smaller initial volatility for $\rho = 0.01$ and $\xi = -0.01$ with $\mu = 0$ at two different stock prices, namely $S = 50(l)$ and $S = 150(l)$. On the same graph, we have also shown the implied volatility curves for the two stock prices, $S = 50(h)$ and $S = 150(h)$ for an initial volatility of unity. We note that the curves can differ significantly for different values of initial volatility. Indeed, when we increase the stock price from 50 to 150, we note that the implied volatilities generally increase for different strike price at the lower initial volatility. However, the reverse effect seems to be taking place when the stock price increase over the same range for a high initial volatility.

Since the results can differ drastically for different initial volatilities, we have also done

graphic7.gif

Figure 15: Volatility curves for different stock price, S . In this simulation, the parameters μ , ξ and ρ have been arbitrarily fixed at 0, 0.01, -0.02.

graphic8.gif

Figure 16: Volatility curves for two stock prices, $S = 50$ and $S = 150$ at different initial volatilities. For the lower initial volatility of 0.2, we have denoted the curves by $S = 50(l)$ and $S = 150(l)$, whereas for the larger initial volatility of 1, we have labeled the curves $S = 50(h)$ and $S = 150(h)$.

some simulation of the implied volatility curves at an initial volatility of 0.2 for different stock prices. Figure 18 and 17 shows the results of our simulation of the implied volatility curves for ξ and μ fixed at 0.01 and 0 respectively. In figure 18, we have considered a positive value of $\rho = 0.01$ whereas in figure 17, we perform the simulation with a negative value of $\rho = -0.03$.

graphic9.gif

Figure 17: Volatility curves for different stock prices between $S = 50$ and $S = 150$ with the initial volatility set at 0.2. The parameters ξ , μ and ρ have been set at 0.01, 0 and -0.03 respectively.

The concavity of the implied volatility curves can significantly affect the decisions of market analysts. In figure 15 and 18, one quickly observes the drastic change in the concavity as the stock prices vary from 50 to 150. In particular, it is interesting to investigate how the implied volatility curves change their concavity between the stock price of 60 and 75 in figure 15. Indeed, figure 15 shows how a smile can turn into a frown if the initial stock price falls from 200 to say 50.

graphic10.gif

Figure 18: Volatility curves for different stock prices between $S = 50$ and $S = 150$ with the initial volatility set at 0.2. The parameters ξ , μ and ρ have been set at 0.01, 0 and 0.01 respectively.

graphic11.gif

Figure 19: Volatility curves for different initial stock prices between $S = 63.1$ and $S = 64.8$ with the parameters fixed at the values for the graph in figure 9. The parameters ξ , μ and ρ have been set at 0.01, 0 and -0.02 respectively.

7 Efficiency of Algorithms

The normal way of doing Monte-Carlo simulations to find option prices with stochastic volatility involves directly simulating the process

$$dS = rSdt + \sqrt{V}SWdt \quad (52)$$

$$dV = (\lambda + \mu V)dt + \xi V^\alpha Qdt \quad (53)$$

by discretising it using the Euler method to

$$\Delta V_i = (\lambda + \mu V_i)\Delta t + \xi V_i^\alpha \epsilon_1 \sqrt{\Delta t} \quad (54)$$

$$\Delta S_i = rS_i\Delta t + \sqrt{V_i}S_i\epsilon_2\sqrt{\Delta t} \quad (55)$$

where the standard normally distributed random variables ϵ_1 and ϵ_2 with correlation ρ are generated by first generating two uncorrelated standard normally distributed random variables δ_1 and δ_2 and using $\epsilon_1 = \delta_1$ and $\epsilon_2 = \rho\delta_1 + \sqrt{1 - \rho^2}\delta_2$. The final values of S are stored and the option price with strike price K is estimated by considering $E[\max(S - K, 0)]$. This is the algorithm used along with the control variate method in Johnson and Shanno [18] (we henceforth call the above algorithm the standard algorithm).

Before we compare the efficiency of our algorithm with the standard one, we look at the possible sources of error and how the error due to each source scales with run time for both. The major source of error for both algorithms is the Monte Carlo error which goes as $N^{-1/2}$ and which goes as the square root of the run time. Another common source of error in both the algorithms is the discretization of the process for y or V . The error in y is then of the order of $h^{1/2}$ where h is the time step used. However, the effect of this

error on the option price is virtually impossible to estimate and we verify that the number of time steps is adequate empirically by comparing two simulations with different numbers of time steps. The standard algorithm has a further error due to the discretization of the S process. The error is again of the order of $h^{1/2}$. The effect of this error on the option price is of the same order as the payoff of the option is piecewise linear with respect to S . Hence, this error also goes inversely as the square root of the run time. Our algorithm has other errors due to the finiteness of the integration over x , the interpolation error and the quadrature error which goes as h^4 . The error due to the finiteness of the quadrature domain can be made completely negligible with minimal effort as the propagator goes as e^{-d^2} where $d = x - x'$. Hence, for large enough d , this error goes as e^{-t^2} where t is the run time. This is a truly negligible error. The interpolation error is difficult to estimate but we empirically show that it is very small for interpolation over 100 points as the propagator is very smooth. The quadrature error goes as h^4 (Simpson's rule). Since most of the computer time is spent on the Monte Carlo simulation, we can also make this error very small with only a small increase in run time. Hence, we see that one of the main advantages of our algorithm is that it has a significantly lower error for the same number of configurations (since it has no error due to the S simulation since these degrees of freedom have been integrated out).

When generating a single set of option prices with the same error tolerance, our algorithm is about 30 times faster. However, our algorithm has an important advantage in that t_1 and t_2 are independent of ρ . Hence, when we generate sets of data with all parameters except ρ fixed, we only need to calculate the new propagator using the terms and integrate over the final payoff. This effectively results in an increase in efficiency of a factor of six to seven when we calculate the prices for 10 different values of ρ . Hence, when generating data with several values of ρ , our algorithm is about two hundred times faster.

At $\alpha = 1$, we can use an alternative algorithm called the bisection method. Compared to usual Monte Carlo methods, the bisection method provides a reasonably fast algorithm for the simulation of derivative pricings. We need to integrate the path integral over x' values. We first divide the interval for the x' values into 100 divisions. For each value of x' , we apply the bisection method and divide the interval y into $2^5 = 32$ points. This application of the bisection method yields one configuration of points. In the algorithm, we sample N such configurations for each value of x' . Using Bode's rule as an integration algorithm, we finally integrate over the x' values. In general, we find that it is sufficient to execute only $N = 100$ configurations for each value of x' in the program since the gain in numerical precision is not

substantial. These results were computed with 100 values of strike prices.

8 Conclusion

The path integral formalism provides an additional tool for analyzing derivative pricing. Although our model may seem heuristic⁸, our techniques and computational method is generally quite novel in the financial market and it has several added advantages. Firstly, it does not assume constant volatility and should be a better tool for analyzing market data. Secondly, the additional parameters clearly allow us to study more carefully the behavior of the volatilities in the market. And lastly, the formalism provides a reasonably fast algorithm for computing the option prices.

In our simulation, we relied on market data to extract the plausible values of μ , α , ρ and ξ . Although the value of ρ in most of the currently well-established markets is believed to hover between -0.5 and 0.5, we did not restrict our ρ to these values. However, it is possible for ρ to assume higher values in more mature markets. Indeed, we have treated our simulation largely as an experimental tool to investigate the qualitative behavior for the implied volatility. We believe that this new formalism, with proper calibration, can offer a formidable tool for getting a more accurate pricing of options. Further, we studied the time period from 90 days to one year and set the initial volatility arbitrarily at unity.

One of the most important qualitative result from our simulations for $\alpha \neq 1$ and $\alpha = 1$ is that at-the-money, the implied volatility is equal to the naive fixed volatility of Black-Scholes, and the latter is approximately equal to the historical volatility. Deep-in-the-money and deep-out-of-the-money show frowns and smiles for implied volatility depends very much on the value of ρ . Finally, the sharp cross-over for the implied volatility for certain special values of initial stock price shows that hedging the option for these values could lead to large changes in the value of the portfolio and can consequently leads to greater risk.

Finally, we emphasize that it is very important to calibrate this path integration model with the market data for different securities and extract all the relevant information about the range of parameters. Such an approach can be extremely interesting and revealing for the traders who would like to have some qualitative ideas regarding the actual behavior of derivative pricing in the markets.

⁸As pointed out by one referee, the issue of the financial market completeness is rather subtle. Allowing trading in stock and riskless bonds implies incompleteness in the market.

9 Endnotes

We are grateful to Lawrence Ma (Man-Drapeau, Singapore) and Choon-Peng Toh (Bank of America) for discussions and helpful conversations. We also thank G. Bhanot for their helpful comments and advices regarding the computational aspect of our work.

Appendix

A A Quantum Mechanical Formulation of the Problem

We define the Hamiltonian operator as

$$\hat{H}(x, y) = - \left(r - \frac{e^y}{2} \right) \frac{\partial}{\partial x} - \left(\lambda e^{-y} + \mu - \frac{\xi^2}{2} e^{2y(\alpha-1)} \right) \frac{\partial}{\partial y} - \frac{e^y}{2} \frac{\partial^2}{\partial x^2} - \rho \xi e^{y(\alpha-1/2)} \frac{\partial^2}{\partial x \partial y} - \frac{\xi^2 e^{2y(\alpha-1)}}{2} \frac{\partial^2}{\partial y^2}. \quad (56)$$

The Hamiltonian is non-Hermitian and accounts for the irreversibility of the stochastic processes in finance. From eq(17), we obtain the Merton-Garman-Schrödinger equation

$$\frac{\partial f}{\partial t} = (r + \hat{H}(x, y))f, \quad (57)$$

$$f(x, y, T) = \max(e^x - K, 0) \quad (58)$$

which can be formally solved as

$$f(x, y, t) = e^{-r\tau} \int_{-\infty}^{\infty} dx' \langle x, y | e^{-\hat{H}\tau} | x' \rangle f(x', T) \quad (59)$$

$$f(x, T) = \max(e^x - K, 0), \tau = T - t$$

While this looks deceptively simple, no analytic solution has been obtained for this equation. The special case $\alpha = \frac{1}{2}$ was solved using a series method by Hull and White [14] and using elementary probability techniques by Heston [13]. the case $\alpha = 1$ was solved by Baaquie [1].

B The Lagrangian for the Problem

The central quantity whose knowledge is sufficient to solve the problem is the conditional probability given by the propagator

$$P(x, y, T | x', t) = \langle x, y | e^{-\hat{H}\tau} | x' \rangle \quad (60)$$

which can be conveniently handled in the Lagrangian formulation of quantum mechanics.

To determine a Lagrangian for the problem, we discretize time so that there are N time steps. The time step is then $\epsilon = \frac{\tau}{N}$. The continuous variables $x(t)$ and $y(t)$ are discretized to x_i and y_i where $0 \leq i \leq N$. The operator $\langle x, y | e^{-\hat{H}\tau} | x', y' \rangle$ can then be decomposed to

$$\begin{aligned} \langle x, y | e^{-\hat{H}\tau} | x' \rangle &= \int_{-\infty}^{\infty} dy' \langle x, y | (e^{-\hat{H}\epsilon})^N | x', y' \rangle \\ &= \int_{-\infty}^{\infty} dx_{N-1} \int_{-\infty}^{\infty} dy_{N-1} \cdots \int_{-\infty}^{\infty} dx_1 \int_{-\infty}^{\infty} dy_1 \int_{-\infty}^{\infty} dy_0 \times \\ &\quad \langle x_N, y_N | e^{-\hat{H}\epsilon} | x_{N-1}, y_{N-1} \rangle \cdots \langle x_1, y_1 | e^{-\hat{H}\epsilon} | x_0, y_0 \rangle \end{aligned} \quad (61)$$

where $x_N = x$, $y_N = y$, $x_0 = x'$ and $y_0 = y'$.

We see that if we can find $\langle x, y | e^{-\hat{H}\epsilon} | x', y' \rangle$, we can find the propagator and hence the option price. Therefore, let us look at this quantity more closely. Before we consider this quantity for the stochastic volatility case, let us consider the Black-Scholes (constant volatility) case as it is simpler and retains the essential features.

In the Black-Scholes case, we only have one variable x (as y is just a constant). We write

$$\langle x | e^{-\hat{H}_{BS}\epsilon} | x' \rangle = N_{BS}(\epsilon) e^{\hat{L}_{BS}\epsilon} \quad (62)$$

where $N(\epsilon)$ is a normalization constant. We see that

$$N_{BS}(\epsilon) = \frac{1}{\sigma\sqrt{2\pi\epsilon}} \quad (63)$$

$$\hat{L}_{BS} = -\frac{1}{2\sigma^2} \left(\frac{\delta x}{\epsilon} + r - \frac{\sigma^2}{2} \right) \quad (64)$$

where $\delta x = x - x'$.

For the stochastic volatility case, we have

$$\begin{aligned} N(\epsilon) e^{\hat{L}\epsilon} &= \langle x, y | e^{-\hat{H}\epsilon} | x', y' \rangle \\ &= \int_{-\infty}^{\infty} \frac{dp_x}{2\pi} \int_{-\infty}^{\infty} \frac{dp_y}{2\pi} \langle x, y | e^{-\hat{H}\epsilon} | p_x, p_y \rangle \langle p_x, p_y | x', y' \rangle \end{aligned} \quad (65)$$

The Hamiltonian in the phase space basis is given by

$$\begin{aligned} \hat{H} &= \frac{e^y}{2} p_x^2 + \xi \rho e^{y(\alpha-1/2)} p_x p_y + \frac{\xi^2 e^{2y(\alpha-1)}}{2} p_y^2 \\ &\quad + \left(\frac{e^y}{2} - r - \frac{\delta x}{\epsilon} \right) i p_x + \left(\frac{\xi^2 e^{2y(\alpha-1)}}{2} - \lambda e^{-y} - \mu - \frac{\delta y}{\epsilon} \right) i p_y \end{aligned} \quad (66)$$

Hence, we have

$$N(\epsilon)e^{\hat{L}\epsilon} = \int_{-\infty}^{\infty} \frac{dp_x}{2\pi} \int_{-\infty}^{\infty} \frac{dp_y}{2\pi} \exp \left(-\epsilon \left(\frac{e^y}{2} p_x^2 + \xi \rho e^{y(\alpha-1/2)} p_x p_y + \frac{\xi^2 e^{2y(\alpha-1)}}{2} p_y^2 \right. \right. \\ \left. \left. - \left(\frac{\delta x}{\epsilon} + r - \frac{e^y}{2} \right) i p_x - \left(\frac{\delta y}{\epsilon} + \lambda e^{-y} + \mu - \frac{\xi^2 e^{2y(\alpha-1)}}{2} \right) i p_y \right) \right). \quad (67)$$

We obtain in a straightforward but tedious manner

$$N(\epsilon) = \frac{e^{y(1/2-\alpha)}}{2\pi\epsilon\xi\sqrt{1-\rho^2}} \quad (68)$$

and

$$\hat{L} = -\frac{e^{2y(1-\alpha)}}{2\xi^2(1-\rho^2)} \left(\frac{\delta y}{\epsilon} + \lambda e^{-y} + \mu - \frac{\xi^2 e^{2y(\alpha-1)}}{2} \right)^2 \\ + \frac{\rho e^{y(1/2-\alpha)}}{\xi(1-\rho^2)} \left(\frac{\delta x}{\epsilon} + r - \frac{e^y}{2} \right) \left(\frac{\delta y}{\epsilon} + \lambda e^{-y} + \mu - \frac{\xi^2 e^{2y(\alpha-1)}}{2} \right) \\ - \frac{e^{-y}}{2(1-\rho^2)} \left(\frac{\delta x}{\epsilon} + r - \frac{e^y}{2} \right)^2 \quad (69)$$

which can be simplified to

$$\hat{L} = -\frac{e^{-y}}{2(1-\rho^2)} \left(\frac{\delta x}{\epsilon} + r - \frac{e^y}{2} - \frac{\rho e^{y(3/2-\alpha)}}{\xi} \left(\frac{\delta y}{\epsilon} + \lambda e^{-y} + \mu - \frac{\xi^2 e^{2y(\alpha-1)}}{2} \right) \right)^2 \\ - \frac{e^{2y(1-\alpha)}}{2\xi^2} \left(\frac{\delta y}{\epsilon} + \lambda e^{-y} + \mu - \frac{\xi^2 e^{2y(\alpha-1)}}{2} \right)^2 \quad (70)$$

This Lagrangian is difficult to deal with analytically and hence we will consider ways to obtain numerical algorithms for the problem.

It should be emphasized that the above Lagrangian is strictly only correct in the limit $N \rightarrow \infty$ and includes terms of order $O(\epsilon)$ and greater apart from the above expression.

C Discretized Version of the Action

The action is defined as

$$S = \int L dt. \quad (71)$$

The discretized version of the action is given by $S = \epsilon \sum_{i=1}^N L_i + O(\epsilon)$ where L_i is the Lagrangian at time step i . The propagator can be written in terms of the action as

$$\langle x, y | e^{-\hat{H}\tau} | x' \rangle = \int_{-\infty}^{\infty} dy' \langle x, y | e^{-\hat{H}\tau} | x', y' \rangle \quad (72)$$

$$= \lim_{N \rightarrow \infty} \int DXDY e^S \quad (73)$$

where we define

$$DX = \frac{e^{-y_N/2}}{\sqrt{2\pi\epsilon(1-\rho^2)}} \prod_{i=1}^{N-1} \int_{-\infty}^{\infty} \frac{dx_i e^{-y_i/2}}{\sqrt{2\pi\epsilon(1-\rho^2)}}$$

$$DY = \int_{-\infty}^{\infty} dy_0 \left(\prod_{i=1}^{N-1} \int_{-\infty}^{\infty} \frac{dy_i e^{y_i(1-\alpha)}}{\xi \sqrt{2\pi\epsilon}} \right)$$

(again $x_0 = x'$, $x_N = x$, $y_0 = y'$ and $y_N = y$). We note that the action is quadratic in x . This enables us to integrate over the stock price.

We define

$$Q = \int DX e^{S_x} = \frac{e^{-y_N/2}}{\sqrt{2\pi\epsilon(1-\rho^2)}} \prod_{i=1}^{N-1} \int_{-\infty}^{\infty} \frac{dx_i e^{-y_i/2}}{\sqrt{2\pi\epsilon(1-\rho^2)}} e^{S_x} \quad (74)$$

which is the integral of the action over the stock price.

We now find Q . The x -dependent term in the Lagrangian is

$$L_x(i) = -\frac{e^{-y_i}}{2(1-\rho^2)} \left(\frac{\delta x_i}{\epsilon} + r - \frac{e^{y_i}}{2} - \frac{\rho e^{y_i(3/2-\alpha)}}{\xi} \left(\frac{\delta y_i}{\epsilon} + \lambda e^{-y_i} + \mu - \frac{\xi^2 e^{2y_i(\alpha-1)}}{2} \right) \right)^2 \quad (75)$$

Let

$$c_i = r - \frac{e^{y_i}}{2} - \frac{\rho e^{y_i(3/2-\alpha)}}{\xi} \left(\frac{\delta y_i}{\epsilon} + \lambda e^{-y_i} + \mu - \frac{\xi^2 e^{2y_i(\alpha-1)}}{2} \right) \quad (76)$$

Hence,

$$S_x = -\frac{1}{2\epsilon(1-\rho^2)} \sum_{i=1}^N e^{-y_i} (x_i - x_{i-1} + \epsilon c_i)^2 \quad (77)$$

We now change the variables to z_i defined by

$$x_i = z_i - \epsilon \sum_{j=1}^i c_j \quad (78)$$

Then,

$$S_z = -\frac{1}{2\epsilon(1-\rho^2)} \sum_{i=1}^N e^{-y_i} (z_i - z_{i-1})^2 \quad (79)$$

obtaining

$$Q = \int DX e^{S_x} = \frac{e^{-y_N/2}}{\sqrt{2\pi\epsilon(1-\rho^2)}} \prod_{i=1}^{N-1} \int_{-\infty}^{\infty} \frac{dz_i e^{-y_i/2}}{\sqrt{2\pi\epsilon(1-\rho^2)}} e^{S_z} \quad (80)$$

All the z_i integrations can be performed exactly by a process of induction. The exact procedure can be found in any textbook on path integration such as Kleinert [20] or Roepstorff [27]. (It is also treated in Baaquie [1]). We illustrate the method below.

The integration over z_1 is easily performed. We obtain

$$\begin{aligned} & \int_{-\infty}^{\infty} \frac{dz_1 e^{-y_1/2}}{\sqrt{2\pi\epsilon(1-\rho^2)}} \exp\left(-\frac{1}{2\epsilon(1-\rho^2)} [e^{-y_2} (z_2 - z_1)^2 + e^{-y_1} (z_1 - z_0)^2]\right) \\ &= \frac{e^{y_2/2}}{\sqrt{e^{y_1} + e^{y_2}}} \exp\left(-\frac{1}{2\epsilon(1-\rho^2)} \frac{1}{e^{y_1} + e^{y_2}} (z_2 - z_0)^2\right) \end{aligned} \quad (81)$$

The above integration can be repeatedly performed over all the variables z_i to obtain

$$Q = \frac{e^{S_1}}{\sqrt{2\pi\epsilon(1-\rho^2) \sum_{i=1}^N e^{y_i}}} \quad (82)$$

where

$$\begin{aligned} S_1 &= -\frac{1}{2\epsilon(1-\rho^2) \sum_{i=1}^N e^{y_i}} (z_N - z_0)^2 \\ &= -\frac{1}{2\epsilon(1-\rho^2) \sum_{i=1}^N e^{y_i}} \left(x - x' + \epsilon \sum_{i=1}^N c_i\right)^2 \\ &= -\frac{1}{2\epsilon(1-\rho^2) \sum_{i=1}^N e^{y_i}} \times \\ & \quad \left[x - x' + \epsilon \sum_{i=1}^N \left\{ r - \frac{e^{y_i}}{2} - \frac{\rho e^{y_i(3/2-\alpha)}}{\xi} \left(\frac{\delta y_i}{\epsilon} + \lambda e^{-y_i} + \mu - \frac{\xi^2 e^{2y_i(\alpha-1)}}{2} \right) \right\} \right]^2. \end{aligned} \quad (83)$$

On taking the limit, $N \rightarrow \infty$, we get

$$S_1 = -\frac{1}{2(1-\rho^2)\omega} \left(x - x' + r\tau - \frac{\omega}{2} - \frac{\rho(e^{y(\tau)(3/2-\alpha)} - e^{y(0)(3/2-\alpha)})}{(3/2-\alpha)\xi} - \frac{\rho\lambda}{\xi}\theta - \frac{\rho\mu}{\xi}\eta + \frac{\rho\xi}{2}\zeta \right)^2 \quad (84)$$

The term $e^{y(0)(3/2-\alpha)}$ arises from the fact that $\int_0^\tau dt e^{y(3/2-\alpha)} \frac{dy}{dt} = \int_{y(0)}^{y(\tau)} dy e^{y(3/2-\alpha)}$ and

$$\omega = \int_0^\tau e^y dt = \int_0^\tau V dt \quad (85)$$

$$\theta = \int_0^\tau e^{y(1/2-\alpha)} dt = \int_0^\tau V^{1/2-\alpha} dt \quad (86)$$

$$\eta = \int_0^\tau e^{y(3/2-\alpha)} dt = \int_0^\tau V^{3/2-\alpha} dt \quad (87)$$

$$\zeta = \int_0^\tau e^{y(\alpha-1/2)} dt = \int_0^\tau V^{\alpha-1/2} dt. \quad (88)$$

Hence, if we can find the joint probability density functions for ω , θ , η , ζ and $\nu = V^{3/2-\alpha}(0)$, with V following the stochastic process in (6), we obtain an analytic solution for the problem given by

$$\langle x, y | e^{-\hat{H}\tau} | x' \rangle = \int_0^\infty d\omega \int_0^\infty d\theta \int_0^\infty d\eta \int_0^\infty d\zeta \int_0^\infty d\nu \frac{e^{S_1(\omega, \theta, \eta, \zeta, \nu)}}{\sqrt{2\pi\epsilon(1-\rho^2)\omega}} f(\omega, \theta, \eta, \zeta, \nu) \quad (89)$$

where f is the joint probability distribution function.

Hence, we retain the discrete solution which finally gives us

$$\langle x, y | e^{-\hat{H}\tau} | x' \rangle = \int DY \frac{e^{S_0+S_1}}{\sqrt{2\pi\epsilon(1-\rho^2) \sum_{i=1}^N e^{y_i}}} \quad (90)$$

$$\equiv \int DYP(x, y, \tau | x', y') \quad (91)$$

where S_1 is given in (83) and

$$S_0 = -\frac{\epsilon}{2\xi^2} \sum_{i=1}^N e^{2y_i(1-\alpha)} \left(\frac{\delta y_i}{\epsilon} + \lambda e^{-y_i} + \mu - \frac{\xi^2 e^{2y_i(\alpha-1)}}{2} \right)^2 \quad (92)$$

$$DY = dy_0 \left(\prod_{i=1}^{N-1} \frac{dy_i e^{y_i(1-\alpha)}}{\sqrt{2\pi\epsilon\xi}} \right) \quad (93)$$

We need to start from the path integral given in eq(73) to study numerically correlators such as $\langle e^{X_n} e^{Y_m} \rangle$. However, if one is interested solely in the price of the option, one needs to determine only $P(x, y, \tau | x', y')$ and in this case, the simplified discrete-time path integral obtained in eq(90) should be used as the starting point for numerical studies.

References

- [1] B. Baaquie, J. de Phys. I, **7** (1997) L733.
- [2] C. Ball and A. Roma, J. Fin. Quant. Analy.,**29** (1994) 589.
- [3] G. Bhanot, C. Lang and C. Rebbi, Comp. Phys. Comm., (1982) 275
- [4] F. Black and M. Scholes, J. Pol. Econ., **8** (1973), 637.
- [5] J. Bodurtha and G. Courtadon, Working Paper, Ohio Sate University, WPS 84-69 (1984)
- [6] J. Bouchaud and G. Lori and D. Sornette, Risk Mag. (1995).
- [7] R. Cameron and W. Martin, J. Math. Phys., **34** (1944) 195.
- [8] R. Cont, M. Potters and J. Bouchaud, Lanl Preprint cond-mat-9705087.
- [9] J. Cox and S. Ross, J. Fin. Econ., **3** (1976) 145.
- [10] J. Cox and M. Rubenstein, *Options Markets* (Prentice Hall, New York, 1985).
- [11] S. Das and R. Sudaram, J. Fin. Quant. Anal. (1999), to appear in June issue.
- [12] T. Finucane, *Fourth Symposium on the Frontiers of Massively Parallel Computers*, Mclean, Virginia.
- [13] S. Heston, The Rev, Fin. Stud., **6** (1993) 327.
- [14] J. Hull and A. White, Adv. Fut. Opt. Res., **3** (1988), 29.
- [15] J. Hull and A. White, J. Int. Money Fin., **6** (1987) 131.
- [16] J. Hull and A. White, J. Fin., **XLII** (1987) 281.
- [17] R. Jarrow and A. Rudd, *Option Pricing* (Irwin, New York, 1983).
- [18] H. Johnson and D. Shanno, J. Fin Quant. Anal., **22** (1993) 143.
- [19] E. Jones, J. Fin. Econ.,**13** (1984) 91

- [20] H. Kleinert, *Path Integrals in Quantum Mechanics, Statistics and Polymer Physics* (World Sci., Singapore, 1990).
- [21] S. Kon, J. Fin., **39** (1984) 147.
- [22] C. Lamoureaux and W. Lastrapes, The Rev Fin. Stud., **6** (1993) 293.
- [23] R. Merton, Bell J. Econ. Management Sci., **4** (1973) 141.
- [24] R. Merton, J. Fin. Econ., **3** (1976) 125.
- [25] K. Mills, M. Vinson and G. Cheng, Syracuse University NPAC Technical Report SCCS-260, 1993.
- [26] M. Potters, R. Cont and J. Bouchaud, Lanl Preprint cond-mat-9609172.
- [27] G. Roepstorff, *Path Integral Approach to Quantum Physics* (Springer Verlag, Berlin, 1991).
- [28] M. Rubenstein, J. Fin., **38** (1983) 213.
- [29] M. Rubenstein, J. Fin., **40** (1986) 445.
- [30] L. Scott, J. Fin Quant. Anal., **22** (1987) 419.

This figure "graphics1.gif" is available in "gif" format from:

<http://arxiv.org/ps/cond-mat/0008327v1>

This figure "graphic2.gif" is available in "gif" format from:

<http://arxiv.org/ps/cond-mat/0008327v1>

This figure "graphic3.gif" is available in "gif" format from:

<http://arxiv.org/ps/cond-mat/0008327v1>

This figure "graphics4.gif" is available in "gif" format from:

<http://arxiv.org/ps/cond-mat/0008327v1>

This figure "graphic5.gif" is available in "gif" format from:

<http://arxiv.org/ps/cond-mat/0008327v1>

This figure "graphic6.gif" is available in "gif" format from:

<http://arxiv.org/ps/cond-mat/0008327v1>

This figure "graphic7.gif" is available in "gif" format from:

<http://arxiv.org/ps/cond-mat/0008327v1>

This figure "graphic8.gif" is available in "gif" format from:

<http://arxiv.org/ps/cond-mat/0008327v1>

This figure "graphic9.gif" is available in "gif" format from:

<http://arxiv.org/ps/cond-mat/0008327v1>

This figure "graphic10.gif" is available in "gif" format from:

<http://arxiv.org/ps/cond-mat/0008327v1>

This figure "graphic11.gif" is available in "gif" format from:

<http://arxiv.org/ps/cond-mat/0008327v1>